138 (2022) 212870

Contents lists available at ScienceDirect

Biomaterials Advances

journal homepage: www.journals.elsevier.com/materials-science-and-engineering-c

A novel multi-target strategy for Alzheimer's disease treatment via sublingual route: Donepezil/memantine/curcumin-loaded nanofibers

Fadime Topal [a,b,1], Busra Ertas [a,1], Ece Guler [a,b], Fatmanur Gurbuz [a], Gul Sinemcan Ozcan [c], Oguzhan Aydemir [d], Veysel Gokhan Bocekci [e], Gokhan Duruksu [c], Cansun Sahin Cam [f], Yusufhan Yazir [c], Oguzhan Gunduz [b,g], Muhammet Emin Cam [a,b,*]

[a] Department of Pharmacology, Faculty of Pharmacy, Marmara University, Istanbul 34854, Turkey
[b] Center for Nanotechnology and Biomaterials Application and Research, Marmara University, Istanbul 34722, Turkey
[c] Stem Cell and Gene Therapies Research and Applied Center, Medical Faculty, Kocaeli University, Kocaeli 41380, Turkey
[d] Department of Research & Development, Joker Food Industry International Domestic and Foreign Trade Company, Istanbul 34885, Turkey
[e] Department of Electrical and Electronics Engineering, Faculty of Technology, Marmara University, Istanbul 34722, Turkey
[f] Department of Psychiatry, Faculty of Medicine, Marmara University, Istanbul 34854, Turkey
[g] Department of Metallurgy and Material Engineering, Faculty of Technology, Marmara University, Istanbul 34722, Turkey

ARTICLE INFO

Keywords:
Alzheimer's disease
Memantine
Donepezil
Curcumin
Electrospun nanofiber

ABSTRACT

Drug delivery systems that not only show efficacy through multiple therapeutic pathways but also facilitate patient drug use and exhibit a high bioavailability profile represent a promising strategy in the treatment of Alzheimer's disease (AD). Here, donepezil (DO)/memantine (MM)/curcumin (CUR)-loaded electrospun nanofibers (NFs) were produced for the treatment of AD. DSC, XRD, and FT-IR studies demonstrated the complete incorporation of the drug into PVA/PVP NFs. The disintegration profile was improved by loading the drugs in PVA/PVP with fast wetting (less than 1 s), the start of disintegration (21 s), and dispersion in 110 s. The desired properties for sublingual application were achieved with the dissolution of NFs in 240 s. The cell viability in DO/MM/CUR-loaded NFs was similar to the control group after 48 h in the cell culture. DO/MM/CUR-loaded NFs enhanced the expressions of BDNF (13.5-fold), TUBB3 (8.9-fold), Neurog2 (5.6-fold), NeuroD1 (5.8-fold), Nestin (166-fold), and GFAP (115-fold). DO/MM/CUR-loaded NFs and powder of these drugs contained in these fibers were daily administered sublingually to intracerebroventricular-streptozotocin (icv-STZ) treated rats. DO/MM/CUR-loaded NFs treatment improved the short-term memory damage and enhanced memory, learning ability, and spatial exploration talent. Results indicated that the levels of Aβ, Tau protein, APP, GSK-3β, AChE, and TNF-α were significantly decreased, and BDNF was increased by DO/MM/CUR-loaded NFs treatment compared to the AD group. In the histopathological analysis of the hippocampus and cortex, neuritic plaques and neurofibrillary nodes were not observed in the rats treated with DO/MM/CUR-loaded NFs. Taken together, the sublingual route delivery of DO/MM/CUR-loaded NFs supports potential clinical applications for AD.

1. Introduction

Alzheimer's disease is a progressive neurological disorder that is caused by many factors such as the accumulation of amyloid plaques and neurofibrillary tangles, neuroinflammation, transmission deficiency, and irreversible neuron loss and consists of pathways that trigger each other [1,2]. It is known that over 50 million people worldwide suffered from AD, and its prevalence is predicted to nearly double by 2050 [3].

Abbreviations: DO, Donepezil; MM, Memantine; CUR, Curcumin; NFs, Nanofibers; AD, Alzheimer's disease; PVP, Polyvinyl pyrrolidone; PVA, Polyvinyl alcohol; XRD, X-ray diffraction; SEM, Scanning electron microscopy; FT-IR, Fourier transforms infrared spectroscopy; ICV, Intracerebroventricular; STZ, Streptozotocin; DSC, Differential Scanning Calorimeter; DP-SCs, Dental pulp stem cells; BDNF, Brain-derived neurotrophic factor; EGF, Epidermal growth factor; bFGF, Basic fibroblast growth factor; IBMX, Isobutyl methylxanthine; GFAP, Glial fibrillary acidic protein; NeuroD1, Neuronal differentiation 1; Neurog2, Neurogenin 2; TUBB3, Tubulin, beta 3; Actb, Actin, beta; P3, Human foreskin fibroblasts; H&E, Hematoxylin and eosin.

* Corresponding author at: Department of Pharmacology, Faculty of Pharmacy, Marmara University, Istanbul 34854, Turkey.
E-mail address: muhammet.cam@marmara.edu.tr (M.E. Cam).

[1] Contributed equally to this work.

https://doi.org/10.1016/j.bioadv.2022.212870
Received 17 November 2021; Received in revised form 7 May 2022; Accepted 14 May 2022
Available online 18 May 2022

This rapid progression of the illness and the decrease in patients' quality of life occasion a serious socio-economic burden on the health systems of developing countries [4]. The AD treatment is carried out with only available two drug groups with symptomatic efficacy: the cholinesterase inhibitors and the glutamate receptor antagonist, which include donepezil (DO) and memantine (MM), respectively [5]. Although the currently used drugs in the treatment of AD regulate the disease symptoms, they cannot prevent the progression of the disease. These drugs, which are administered to patients via oral in tablet, capsule, and suspension forms, undergo the hepatic first-pass effect, and hence, their bioavailability decreases [6,7]. Curcumin (CUR) is a natural polyphenol product obtained from the rhizome of *Curcuma longa,* CUR has been proven by many studies to have a protective effect on neurons along with its strong antioxidant properties [8]. In addition, curcumin displays neuroprotective properties by inhibiting amyloid β oligomerization and tau-phosphorylation by demolishing amyloid-β precursor protein. Despite its known therapeutic activity, it is stated that hydroxyl groups in the structure of curcumin cause it to become unstable in biological terms. Therefore, although curcumin crosses the blood-brain barrier, it has low brain bioavailability due to its rapid metabolism [9].

Increasing evidence indicates that a restrictive effect on disease progression is not possible with a drug targeting a single stage of the pathology [6]. In addition, studies report that in addition to the many limitations of single-drug therapy, including safety, efficacy, and disease management in AD treatment, the fact that efficacy is only possible with high doses causes patients to have to cope with side effects [10]. In recent years, studies have focused on developing combined drugs targeting multiple pathways to overcome the multifaceted pathogenesis of the disease [11]. Combined therapies targeting different therapeutic pathways show better efficacy compared to the monotherapy [12]. Moreover, combined forms of drugs are an innovative approach to current problems in the treatment of AD, by enabling lower doses, fewer side effects, and costs compared to their single forms. Based on the literature, studies investigating methods that allow the combined use of drugs with known efficacy has an important place in the treatment of AD due to their analytical approach to existing problems [13].

Nanotechnology is developing rapidly as one of our age's most important research and application areas [14]. Various potential drug development initiatives in the form of drug delivery systems such as nanoparticles, liposomes, and nanofibers (NFs) are important to provide a multifaceted effect on the disease by increasing drug bioavailability in the AD treatment [15,16]. Electro-spinning is an easy and cost-effective method that is frequently preferred to produce nanofibers with a suitable pore structure and a large surface area in the desired diameter scale [17–19]. Electrospun-NFs are frequently preferred drug delivery systems due to their advantages, such as imitation of the natural extracellular matrix, high-density pores, high-surface volume ratio, high permeability, low weight, and small-fiber diameter. In addition to all these, it is an important advantage that it offers the opportunity to collect the combination of many drugs in one form [20,21]. It is also known that AD patients may miss doses of their regimen due to their illness, may not want to take medication, and/or may have difficulty swallowing [22]. For this reason, the sublingual use of drug-loaded nanofibers is considered to be a factor that increases patient compliance, providing accurate dosing and easy administration. Polymers such as hydrophilic polyvinyl alcohol (PVA), polyvinyl pyrrolidone (PVP), polyethylene glycol, poly (acrylic acid), and chitosan have been extensively utilized to produce fibers with fast released properties via sublingual route [23–26].

Herein, we investigated the effect of DO, MM, and CUR-loaded nanofibers (DO/MM/CUR-loaded NFs) on neuronal differentiation and its neuroprotective effect through multiple therapeutic pathways compared to their single-use. For the first time, the efficacy of sublingual use of DO/MM/CUR-loaded nanofibers along with anticholinesterase effect, glutamate receptor antagonism, and mechanisms preventing the accumulation of amyloid-β was elucidated in this study. For this purpose, a PVA/PVP polymer blend in fiber production has been optimized, and DO, MM, and CUR have been loaded into the optimized polymer blend, which exhibits the best morphology. In addition, the physical parameters of the polymer blend were evaluated. The crystalline, morphological, and chemical properties of all electrospun fibers were examined using X-ray diffraction (XRD), Scanning electron microscopy (SEM), and Fourier transforms infrared spectroscopy (FT-IR), respectively. The mechanical and thermal properties of the fibers were analyzed. A dissolution test was carried out after wetting and disintegration tests to examine the fibers' fast release property. The effects of NFs on stem cell differentiation and neuronal cell markers and their cytotoxic effects were examined in cell culture. After that, an Alzheimer's model was created in rats by intracerebroventricular-streptozotocin (icv-STZ) administration, and the neuroprotective effect of electrospun fibers was evaluated by biochemical, histological, and behavioral analysis (see Fig. S1 in the article's Supporting Information for a schematic illustration of the methods).

2. Materials and methods

2.1. Chemicals

Donepezil (DO, Mw ~ 379,492 g/mol) and memantine (MM, Mw ~ 179.3 g/mol) were kindly provided by Sanovel Pharmaceutical (Istanbul, Turkey) and Deva Holding (Istanbul, Turkey). Polyvinyl alcohol (PVA, Mw ~ 89,000-98,000), polyvinyl pyrrolidone (PVP, Mw ~ 40,000), ethanol (%99.9 purity, *v*/v) were purchased from Sigma-Aldrich (UK). Streptozotocin was obtained from Santa Cruz Biotechnology, Inc. (Dallas, TX, USA). All purchased materials are of analytical grade.

2.2. Methods

2.2.1. Preparation of curcumin

Curcuma longa rhizomes from Istanbul, Turkey were used. *Curcuma longa* rhizomes were screened and sieved after being dried at 105 °C for three hours in an oven. After obtaining dried *Curcuma longa* rhizomes, the Soxhlet extraction process was applied as follows (Supporting Information, Fig. S2): Acetone was utilized as the extraction solvent and added to 15 g of dried and sieved *Curcuma longa* rhizome, which was weighed in a flask. The Soxhlet extraction was applied for eight hours at 60 °C. Subsequently, the solvent was separated from the residue and evaporated under a vacuum at 35 °C to obtain a dry *Curcuma longa* rhizome extract [27].

2.2.2. Preparation and characterization of solutions

PVA (15%, *w*/v) and PVP (15%, *w*/v) were dissolved in a mixture of water: ethanol (4:1) in the present study. PVA/PVP was mixed 7:3, 5:5, and 3:7 (*v*/v) ratios, respectively. SEM images of all pure fibers were examined, and beadless and uniform morphology was obtained in 7:3 (PVA/PVP) ratio. Therefore, MM (12.6 mg/mL, *w*/v) [28], DO (12.6 mg/mL, *w*/v) [29], and CUR (12.6 mg/mL, *w*/v) [30] were added into PVA/PVP (7: 3) composite solution.

The physical parameters of all polymer solutions such as electrical conductivity, surface tension, density, and viscosity were evaluated by an electrical conductivity probe (Cond 3110 SET 1, WTW, Germany), force tensiometer (Kruss K9, Hamburg, Germany), density bottle (10 mL specific density bottle, Boru Cam Inc., Turkey), and DV-E viscometer (Brookfield AMETEK, USA), respectively. All the measurements were repeated three times at 25 °C temperature. Equipment was calibrated before measurements [31].

2.2.3. Electrospinning

Pure and drugs-loaded fibers were made by the electrospinning method at different voltages, the working distances (distance between the needle tip and metal plate), and flow rate. The working distance was

set as 150 mm, the applied voltage was between 19 and 26 kV, and the flow rate was between 0.1 and 0.4 mL/h. The polymer solution was deposited at a 24 kV voltage for the 7:3 (v/v) ratio. The polymer solution was delivered from the syringe to the needle tip by a syringe pump, and the flow rate of the syringe pump was pegged at 0.1 mL/h. SEM was utilized to investigate the diameters and morphology of the fibers, and characterization of the fibers was performed. The process control parameters used for fiber making are given in Table 1.

2.2.4. Scanning electron microscopy (SEM)

The diameter and morphology of the fibers were investigated by SEM (EVO LS 10, ZEISS instrument). Before SEM, the surface of all samples was covered with gold for 1 min. Mean fiber size distribution and diameter were determined by measuring 100 fibers diameter in randomly selected micrographs using ImageJ software (Brocken Symmetry Software) [32].

2.2.5. Fourier transform İnfrared spectroscopy (FT-IR)

It was used a Jasco FT-IR 4700 spectrometer, and spectrographs were displayed via OPUS Viewer version 6.5 software for FT-IR measurements. Powder of all components within the DO/MM/CUR-loaded NFs content and fiber samples was analyzed to confirm the presence of these materials in fiber samples.

2.2.6. X-ray powder diffraction (XRD)

The crystalline fiber form was determined, composite XRD analysis was reported on a D/Max-BR diffractometer (RigaKu, Japan), and the XRD computer software was used for the analysis [33].

2.2.7. Differential scanning calorimeter (DSC)

Examination of the thermal properties of fibers was performed with a Jade DSC and Pyris software (PerkinElmer Inc., Mass., USA) under a dynamic argon atmosphere (20 mL/min). The temperature borderline was from 25 to 350 °C. This procedure was achieved at a heating rate of 10 °C/min. The thermal properties of the fibers were determined and calibration of the enthalpy and temperature for the DSC was made with pure indium.

2.2.8. Mechanical properties of the fibers

Three samples (10 × 50 mm) were examined for each fiber, and the thickness of the fibers was analyzed utilizing a Mitutoyo digital micrometer (MTI Corp., USA). The tensile strength of the fibers was measured with an Instron 4411 tensile tester at ambient temperature. Both ends of each fiber were clamped with the upper and lower handles. Fibers were exposed to a tensile test with a grip distance of 10 mm and a pull speed of 5 mm min^{-1}. Bluehill 2 software (Elancourt, France) was used for analyzing results [34].

2.2.9. Disintegration and wetting test

30 mm diameter circular section was cut from the fiber using a biopsy cutter and placed in a Petri dish containing 15 mL of simulated saliva (pH 6.8). The formulation for the artificial saliva used in the present study was (wt. percent) potassium phosphate 0.034%, methylparaben 0.2%, sodium carboxymethylcellulose 0.5%, magnesium chloride 0.005%, potassium chloride 0.062%, dextrose 4.69%, and sodium fluoride 0.01% [35]. Magnesium chloride, methylparaben, and dextrose were dissolved in warm water. Then this solution was cooled down before mixing the solutions at ambient temperature. The fibers' disintegration and wetting were recorded at 50 frames per second by a video camera (Canon Sx70 HS, Tokyo, Japan).

2.2.10. Dissolution test

A modified dissolution test was made using a 10 mm long magnetic stirrer in a 70 mm diameter glass Petri dish. 15 mL of simulated saliva at 37 °C was mixed up in a Petri dish at 150 rpm on a multi-point stirrer. 1 mL of the supernatant was transferred to the microtube at predetermined time points and altered with 1 mL of pre-warmed simulated saliva to ensure that the experiment is performed with a constant volume. Experiments were repeated in triplicate.

2.2.11. In vitro release kinetic test

The change in plasma concentration of the drugs in the body over time was simulated *in vitro* and the release of the drugs from the fibers was calculated using five different mathematical models. The equations given below include variables belonging Korsmeyer-Peppas (Eq. (1)), zero-order (Eq. (2)), first-order (Eq. (3)), Higuchi (Eq. (4)), and Hixson-Crowell (Eq. (5)) models [33]. The kinetic constants of these models are K, K_0, K_1, K_h, and K_{hc}, respectively. Q is the fractional amount of drug release at time t. *n* indicates the diffusion exponent.

$$Q = Kt^n \quad (1)$$

$$Q = K_0 t \quad (2)$$

$$\ln(1 - Q) = -K_1 t \quad (3)$$

$$Q = K_h t^{1/2} \quad (4)$$

$$Q^{1/3} = K_{hc} t \quad (5)$$

2.2.12. Effect on stem cell differentiation

To analyze the effects of pure fiber and drug-loaded fibers on the neuronal cell lines, dental pulp stem cells (DP-SCs) originating from neural crest lineage were differentiated into the neuronal neuroglial cell lines *in vitro*. Stem cells used in this study were isolated previously (Karaoz et al., 2011). DP-SCs (P3) were cultured in DMEM supplemented with 1% penicillin-streptomycin (Gibco) and 10% FBS (Gibco) at 37 °C in a humidified atmosphere with 5% CO_2. After reaching 70–80% of cells' confluency, cells were separated by 0.25% trypsin-EDTA (Gibco). The culture medium was refreshed once every 2–3 days.

For neurogenic differentiation, the culture medium was replaced with a differentiation medium which consists of DMEM media supplemented. DMEM was prepared with 0.5 mM isobutyl methylxanthine (IBMX, Sigma–Aldrich, St. Louis, MO), 10 ng/mL brain-derived neurotrophic factor (BDNF), epidermal growth factor (EGF, Biological Industries, Kibbutz Beit Haemek, Israel), basic fibroblast growth factor (bFGF, Sigma–Aldrich), 1% penicillin-streptomycin, and neural stem cell proliferation supplements (Stem Cell Technologies Inc., Vancouver, British Columbia, Canada). Cells were then cultured for seven days in a differentiation environment that was renewed every 2–3 days.

2.2.13. Expression of neuronal cell markers

The expression of some neuronal markers was assessed after culturing DP-SCs with fibers and comparing the results of the gene expression on cell culture in the culture medium without fibers (control). Total RNA was extracted by Aurum Total RNA Mini Kit (BioRad, Hercules, CA) according to the protocol supplied by the manufacturer. cDNA was synthesized by iScript cDNA Synthesis Kit (BioRad) considering the manufacturer's instructions. The gene expression levels (Table 2) were measured by using iTaq Universal SYBR Green Supermix (BioRad) in LightCycler 480-II (Roche). PCR amplification followed a two-step cycling program: 30 s pre-denaturation at 95 °C, 45 cycles of 95 °C for 15 s, and 60 °C for 60 s. Cp values were determined by LightCycler 480 Software (release 1.5), and a melt curve analysis was conducted to evaluate the specificity of the reaction. ActB gene amplification was used as a housekeeping gene in the calculations.

2.2.14. WST assay

To conduct the assay nanofibers were placed into Eppendorf tubes and incubated into DMEM for 24 h at 37 °C. Then, the obtained soluble solutions were used as a conditioned medium to evaluate the nanofiber effects. Human foreskin fibroblasts (P3) were placed into individual

Table 1
Flow rate, voltage, and working distance for different concentrations of PVA/PVP blends and drug-loaded PVA/PVP (7:3) solution.

Solutions (v/v)	Flow rate (mL/h)	Voltage (kV)	Working distance (mm)
PVA/PVP (3:7)	0.3	19	150
PVA/PVP (5:5)	0.4	26	150
PVA/PVP (7:3)	0.1	24	150
PVA/PVP (7:3) + Drugs	0.1	24	150

wells of a 96-well plate (10,000 cells/cm^2) and incubated into DMEM for 24 h in a humidified incubator with 5% CO_2 at 37 °C. After 24 h, the spent medium of the fibroblasts was discarded, and the conditioned medium was added and incubated for 48 h at 37 °C. After seeding on substrates, cell viability was assessed using the WST-1 cell proliferation assay (Roche, Mannheim, Germany) according to the manufacturer's instructions. WST-1 reagent was incubated with standard cell media at 1:10 dilution for 4 h at 37 °C. The WST-1 reagent was then added to each well and was allowed to react with viable cells for 2–3 h. Cleavage of tetrazolium salt in the reagent yields a soluble formazan dye whose rate of production is related to mitochondrial activity. It was also measured its absorbance at 450 nm. The absorbance values of samples were correlated with a standard curve, and cell viability was evaluated as a percentage.

2.2.15. In vivo test

Forty-eight healthy adult male Sprague-Dawley rats (250–350 g) were supplied from the Marmara University Experimental Animal Application and Research Center. Rats were kept in rooms which have been accepted to have appropriate laboratory conditions. Throughout the experiment, the animals were kept in plexiglass cages and provided unlimited feed and water access. All the procedures maintained within the scope of the experiment were carefully implemented by the institutional principle and were carried out in full compliance with an approved protocol (permission no: 76.2019.mar) by the Marmara University Animal Experiments Local Ethics Committee.

2.2.15.1. Experimental design of in vivo testing. Forty-eight rats were randomly divided into four experimental groups, each containing 12 animals. Group 1 (Sham group): The animals in this group were given a bilateral icv injection of saline (5 μL/site/rat), and pure fiber treatment was applied for 21 days. Group 2 (AD group): The animals received a bilateral injection of STZ (5 μL/site/rat), as in the stereotaxic surgery procedure described in the next section, pure fiber treatment was applied for 21 days. Group 3 (DO/MM/CUR-loaded NFs group): Icv injections of STZ and DO/MM/CUR-loaded NFs (5 mg/kg DO [29], 5 mg/kg MM [28], and 5 mg/kg CUR [30] loaded PVA/PVP NFs) were applied via sublingual for 21 days. Group 4 (DO/MM/CUR powder group): Icv injections of STZ and DO/MM/CUR powder (5 mg/kg DO, 5 mg/kg MM, and 5 mg/kg CUR in distilled water) were applied via intra-gastric gavage for 21 days. The dosage amounts of the drugs given orally and sublingually were set to be the same.

The treatment began three days after the operation to minimize the anxiogenic effect of surgical intervention on animals and evaluate their locomotion [36]. Behavioral tests were started on the 11th day of the experimental procedure. After all, *in vivo* experiments were performed, and all animals were euthanized by decapitation (Supporting Information, Fig. S3).

Open field test (OFT), novel object recognition test (NORT), passive avoidance test (PAT), Morris water maze (MWM) test, MWM software analysis program, and software analysis system were given comprehensively in the Supporting Information Materials and Methods section.

2.2.15.2. Intracerebroventricular injection of streptozotocin. The animals were anesthetized with ketamine (100 mg/kg) and xylazine (10 mg/kg) intraperitoneally, placed on a stereotaxic apparatus, and the skull was exposed. Stereotaxic coordinates (as anterioposterior−0.8 mm, lateral 1.5 mm, and dorsoventral-3.6 mm relative to bregma) corresponding to the lateral ventricle were studiously measured and marked [37]. These marked points were opened in the form of holes with fine-tipped dental drills as shown in Fig. S3 (in Supporting Information). A 28-gauge Hamilton syringe was carefully lowered manually through this skull hole to access the lateral ventricle. STZ (3.0 mg/kg; 5 μL/injection site) was injected slowly into each lateral ventricle for 5 min. The same procedures were performed for the sham group, but saline (0.9%) injection was used instead of STZ [38,39].

2.2.16. Biochemical analysis

After their brains were removed to determine biochemical parameters, the hippocampus tissues were rapidly removed and excised. Tissues were homogenized with IKA brand Ultra-Turrax T25 (USA) homogenizer in cold and fresh PBS solution. It was obtained a 10% (*w*/v) homogenate solution. After these samples were centrifuged at 3000 *g* for 10 min, their supernatants were carefully removed and placed at −80 °C for biochemical analysis. Hippocampal Aβ, Tau, APP, GSK-3β, AChE, BDNF, and TNF-α levels were estimated using rat ELISA kits purchased from Bioassay Technology Laboratory, Korain Biotech Co., Ltd. (Shanghai, China). The processes were performed according to the manufacturer's instructions.

2.2.17. Histopathological analysis

The brain tissues of animals were harvested and fixed in 10% neutral buffered formalin for at least 48 h. After fixation, tissue samples were dehydrated in four graded ethanol series (70, 90, 96, and 100%), cleared in xylene, and embedded in paraffin. Histological analysis was made using tissue fragments (4 μm-thick) dyed with hematoxylin and eosin (H&E). Sections were then examined by light microscopy (LEICA DM 1000) and photographed.

2.2.18. Immunohistochemistry

Immunohistochemistry investigation of β-amyloid and Tau protein was performed. The sections which were obtained from animals were deparaffinized, next immersed in 3% H_2O_2 for suppression of endogenous peroxidase activity. After that, it was microwaved in 10 mM sodium citrate at pH 6.0 for 20 min for antigen retrieval. Then, avidin and biotin were added to remove endogenous biotin-related background staining. The sections were then incubated with primary antibodies (anti-β-amyloid (ABCAM, ab10148) and anti-Tau (ABCAM, ab131354)) or PBS (negative control) at 4 °C overnight and incubated, respectively, with a biotinylated secondary antibody and HRP-conjugated streptavidin (ABCAM, ab236466) for quarter-hour at 25 °C temperature. The slides were washed, and the chromogen was developed for 5 min with liquid 3,30-diaminobenzidine before observation. Contrasting staining with hematoxylin was performed. The expression of both primary antibodies was photographed under light microscopy.

For scoring, anti-tau and anti-beta amyloid expression were examined under light microscopy at x40 magnification and evaluated in 5 areas from each rat's section and scored semi-quantitatively from 0 to 3 (none, 0; some, 1; moderate, 2; or extensive, 3). In a case scored 1, occasional positively stained fibrils were seen; for score 2, several stained fibrils were noted with additional threads, and for score 3, numerous fibrils and threads were noted [40].

2.2.19. Statistical analysis

Statistical analysis of the data, which were results from the tests and analysis, was made by GraphPad Prism 8.0 statistical program. Results were quoted as mean ± standard error of the mean except for fiber distribution graphs, which were offered as mean ± standard deviation. Inter-group evaluations were made by analysis of variance (ANOVA) and Tukey post hoc test. $p < 0.05$ values were deemed meaningful.

Table 2
Primer list of neuronal markers for gene expression analysis.

Gene name	Forward sequence (5′-3′)	Reverse sequence (5′-3′)
Brain-derived neurotrophic factor (BDNF)	gagctgagcgtgtgtgacag	gcaaaaagagaattggctggcg
Glial fibrillary acidic protein (GFAP)	tcctcaggggagatgatggt	ttctcgatgtagctggcaaag
Nestin	ctctgacctgtcagaagaat	gacgctgacacttacagaat
Neuronal differentiation 1 (NeuroD1)	gttatgagactatcactgctcaggacc	agaagttgccattgatgctgagc
Neurogenin 2 (Neurog2)	atccgagcagcactaacacg	gctgaggcacagttagagcc
Tubulin, beta 3 (TUBB3)	catggacagtgtccgctcag	caggcagtcgcagttttcac
Actin, beta (Actb)	tggcaccacaccttctacaatgagc	gcacagcttctccttaatgtcacgc

3. Results

3.1. Optimization process and solution characterization

Three different conditions are essential for the optimization of the fibers produced by electrospinning. The first condition is the ambient conditions that require temperature and humidity control; the second condition is the operating conditions (working distance, needle diameter, flow rate of the polymer blend, and an applied voltage); the third condition is the properties of a solution such as solvent, density, electrical conductivity, viscosity, and surface tension.

The physical parameters of the solutions changed with the loading of drugs on composites. Surface tension, viscosity, and density increased by adding drugs from 52 mN/m to 140 mN/m, from 5890 mPas to 12,930 mPas, and from 1.007 g/mL to 1.024 g/mL, respectively. Unlike these physical parameters, electrical conductivity decreased from 393 μS/cm to 304 μS/cm (Supporting Information, Fig. S5).

3.2. Morphological characterization of fibers

The diameter and morphology of pure and drugs-loaded fibers were analyzed using SEM imaging. At 3:7 (PVA/PVP, *v*/v) blend ratio beads were observed, and no fiber formation occurred. Fig. 1 shows that fibers were formed in the other two blend ratios, but the fiber diameter distribution of the two ratios was different. While fiber formation was observed in the 5:5 (*v*/v) mixture, the number of beads present was also high. The fiber with the best morphology was acquired at a 7:3 (*v*/v) blend ratio for PVA/PVP mixture. Therefore, CUR, MM, and DO were loaded to this blend ratio.

The diameters of pure PVA/PVP fibers at 5:5 and 7:3 (*v*/v) blend ratios are 96 ± 25 nm and 189 ± 39 nm, respectively. The diameter of DO/MM/CUR-loaded PVA/PVP (7:3, *v*/v) NFs is 631 ± 132 nm. When the SEM results were evaluated, it has been seen the diameter of DO/MM/CUR-loaded PVA/PVP (7:3) NFs increased compared to pure fiber due to increased viscosity and surface tension of drugs-added solution compared to pure solution.

3.3. Fourier-transform infrared spectroscopy (FT-IR)

FT-IR spectra of pure MM, DO, CUR, PVA, PVP, pure PVA/PVP NFs, and DO/MM/CUR-loaded NFs are shown in Supporting Information, Fig. S6. FT-IR spectra exhibited characteristic absorption peaks of pure DO at 3585.00, 3361.32, 2921.63, 2857.99, 1681.62, and 1066.44 cm^{-1} [41]. These characteristic bands are attributed to -OH group, N—H bond, asymmetric and symmetric C—H bond of the methyl group, C═O bond, and C—O bond stretching, respectively. C—H stretching bands between 2975.62 and 2836.77 cm^{-1} are characteristic absorption peaks of MM [42]. -OH stretching vibration at 3232.11 cm^{-1}, -CH_3 stretching vibration at 2906.20 cm^{-1}, and C—O stretching vibration at 1024.02 cm^{-1} are characteristic peaks of CUR [43]. OH stretching vibration at 3438.46 cm^{-1}, -CH_3 stretching vibration at 2943.80 cm^{-1}, C═O stretching vibration at 1654.62 cm^{-1}, and C—O stretching vibration at 1016.30 cm^{-1} are peaks of PVP [44]. -OH stretching vibration at 3271.64 cm^{-1}, -CH_3 stretching vibration at 2909.09 cm^{-1}, C═O stretching vibration at 1712.48 cm^{-1}, C—O stretching vibration at 1020.16 cm^{-1} are peaks of PVA [45]. A strong absorption peak at 1652.70 cm^{-1} and a broad peak at 3286.11 cm^{-1} belong to the carbonyl (PVP) and hydroxyl stretching (PVA) groups in DO/MM/CUR-loaded NFs, respectively, were shown in the Supporting Information, Fig. S6. The absorption band at 1731.76 cm^{-1} in the spectrum belongs to DO/MM/CUR-loaded NFs and is associated with the stretching vibrations of the C═O group in the structure of DO, while the C = O stretching vibration belongs to CUR is seen at 1498.42 cm^{-1}. For MM, the characteristic peaks have been observed at 2890 cm^{-1} for C—H bond stretching.

3.4. X-ray powder diffraction

XRD was used for the examination of the crystalline structure of samples. The XRD patterns for pure PVA, PVP, CUR, MM, DO, pure PVA/PVP NFs, and DO/MM/CUR-loaded PVA/PVP NFs were given in Supporting Information, Fig. S7. PVP is an amorphous polymer. Diffraction peaks of PVP were detected at 19.81° and 44.0° (Supporting Information, Fig. S7-e) [46]. The XRD pattern of pure PVA has been observed at 2θ = 21.2°, 38.73°, and 44.0° in Supporting Information, Fig. S7-d [47]. XRD patterns of pure PVA and PVP were also seen in pure PVA/PVP composite fiber at 2θ = 19.81°, 21.2°, 38.73°, and 44.0° (Supporting Information, Fig. S7-f). The high density of the XRD pattern at 44.0° is the result of the joining of the peaks belonging to PVA and PVP polymers. Major peaks of MM, DO, and CUR were observed at 2θ = 17.26° due to their crystal nature (Supporting Information, Fig. S7-a) [48], at 2θ = 23.6° (Supporting Information, Fig. S7-b) [49], and at 2θ = 17.36° (Supporting Information, Fig. S7-c) [50], respectively. There are a lot of multiples of CUR peaks in the region 2θ = 5° to 80°. That showed the crystalline nature of the drug. Compared to pure fibers, at 17.26°, 17.36°, and 23.6° peaks were observed in DO/MM/CUR-loaded PVA/PVP NFs and belong to the drugs (Supporting Information, Fig. S7-g).

3.5. Thermal properties of composite nanofibers

DSC was used to analyze the thermal characteristics of pure and drugs-loaded PVA/PVP NFs. The DSC curves of pure PVA/PVP and DO/MM/CUR-loaded PVA/PVP NFs samples are given in Figs. S8a and S8b, respectively. PVP is amorphous, whereas PVA has a crystalline structure. As a result, a slight decrease in values of Tg and melting temperature (Tm) was observed by adding drugs to their blends. The Tg value for pure fibers is 62.9 °C, while it is 60.7 °C for drugs-loaded fibers. The Tm value of pure fibers was 225.1 °C, but the Tm value for drugs-loaded fibers was not seen clearly (Supporting Information, Fig. S8a, and S8b). Besides, the Tm curve of CUR and MM were observed at 178,9 °C and 259.8 °C, respectively (Supporting Information, Fig. S8b) [48]. At the same time, when the results of SEM were examined, it is evident that the fiber diameter of DO/MM/CUR-loaded NFs with low Tg value was larger than the fiber diameter of pure NFs with high Tg value.

3.6. Tensile properties of composite nanofibers

Strain at break and tensile strength of three samples from each of pure PVA/PVP and drugs-loaded PVA/PVP NFs were examined, and an average was taken (Supporting Information, Fig. S9). The tensile strength of pure PVA/PVP NFs is 195 ± 90 kPa, and it decreased to 112 ± 30 kPa by adding drugs to NFs (Supporting Information, Fig. S9a). The strain at the break of pure fibers is 33.6 ± 2.4%, and it increased to 57.5 ± 15.2% by adding drugs (Supporting Information, Fig. S9b). Stress and strain curves were given in Supporting Information, Fig. S9c.

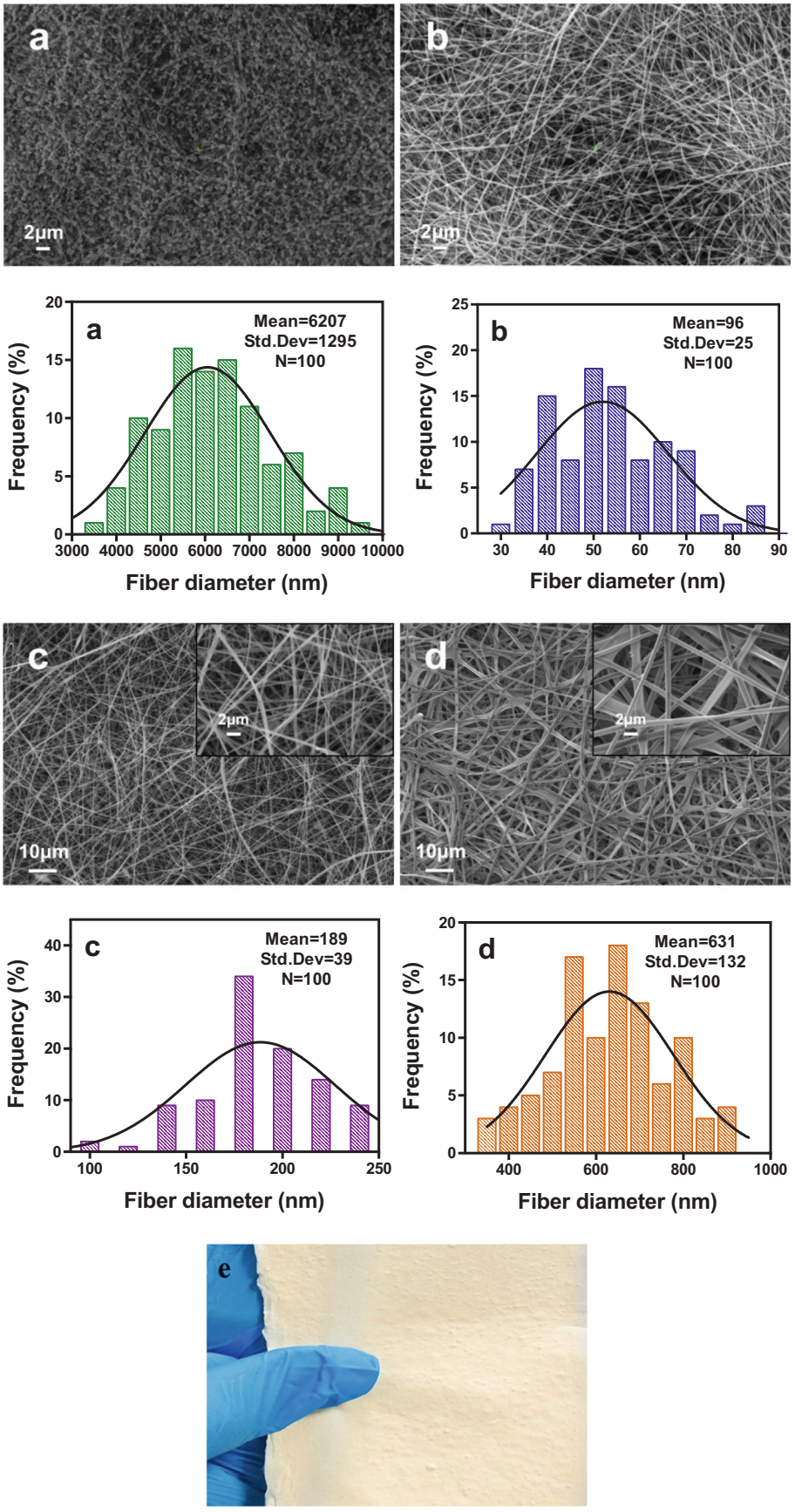

Fig. 1. SEM images and diameter distribution graph of the pure PVA/PVP fibers at three different ratios: (a) 3:7, (b) 5:5, and (c) 7:3 (*v*/v) and drugs-loaded PVA/PVP fibers (7:3, *v*/v) (d), and optical images of DO/MM/CUR-loaded PVA/PVP fibers (e).

3.7. Disintegration and wetting test

30 mm diameter circular sections were cut to measure the wetting and disintegration times of DO/CUR/MM-loaded NFs. The circular section was gently put in simulated saliva. It was observed that fibers quickly became wet in less than 1 s and started disintegration in 21 s and dispersed in almost 110 s in the simulated saliva (Fig. 2).

3.8. Dissolution test

The dissolution profiles of DO, MM, and CUR were examined by UV-spectroscopy by taking the supernatants of DO/MM/CUR-loaded NFs at certain times in the simulated saliva. DO and MM dissolution rates were similar throughout the test period. The percent dissolution rates of DO, MM, and CUR with the supernatant taken at the 60th second of the test were determined as 54.9, 55.4, and 32.7%, respectively. Although CUR's dissolution profile was less than other drugs till 180 s, it was observed that all drugs loaded in fibers dissolved completely at 240 s in simulated saliva (Fig. 3). Moreover, the encapsulation efficiencies within DO/MM/CUR-loaded NFs were calculated as 81.5%, 87.7%, and 71,2% for DO, MM, and CUR, respectively. Since the average encapsulation efficiency was found to be 80%; and knowing that calculating the dose considering that all drugs were encapsulated with an efficiency of 80%, will not lead to a toxic dose or loss of effect in the given drugs; the encapsulation efficiency of all drugs to be given to the animal in NFs was accepted as 80% and the amount of NFs given to rats was calculated according to this ratio and they were given according to the bodyweight of animals.

3.9. In vitro release kinetic test

Mathematical modeling of drug release kinetics plays a significant role in the analysis of the drug release kinetics [51]. Five different mathematical models were used to analyze the release kinetics of drugs being in DO/MM/CUR-loaded NFs. Regression coefficients (R^2) and kinetic constants of these models were given in Table 3, and the details of the models were given in Fig. 4. According to the R^2 values, CUR provided the best compliance with the Korsmeyer-Peppas, while DO and MM were in better agreement with the Higuchi model.

The n values of Korsmeyer-Peppas are 0.8555, 0.8423, and 0.8435 for CUR, DO, and MM, respectively. It was known that when $0.45 \leq n$, the drug release was by Fickian diffusion, and when $0.45 < n < 1$, the drug release was by non-Fickian diffusion [52]. Since all n values were higher than 0.45, it was understood that the drug release was via the non-Fickian diffusion model.

3.10. Cell culture and differentiation

The effects of both DO/MM/CUR-loaded and pure PVA/PVP NFs were evaluated *in vitro* by the culture of DP-SCs in the culture medium and the neurogenic differentiation medium, separately. Despite the reduced viability of fibroblast cells, DP-SCs seemed more resistant to the effect of released DO/MM/CUR from NFs. The number of surviving cells on DO/MM/CUR-loaded NFs was much lower than that of pure NFs. After 7 days, DP-SCs cultured on both pure NFs and drugs-loaded NFs did not differentiate into neuronal or neuroglial cells (Fig. 5a). These cells on pure NFs demonstrated slightly improved expression of BDNF (1.4-fold compared to control), without the need for any chemical induction to differentiate. Cells cultured in a standard medium with DO/MM/CUR-loaded NFs significantly induced the expression of Nestin (13.4-fold), NeuroD1 (3.6-fold), and GFAP (18-fold) compared to the control culture.

3.11. Expression of neuronal cell markers

The stem cells were induced to differentiate into neuronal cells by the defined chemical cocktail under the culture conditions. The results indicated that this chemical cocktail significantly enhanced the neuronal differentiation of DP-SCs. Under the effect of this induction, pure NFs improved the expression of neuronal markers: BDNF (3.7-fold), TUBB3 (6.4-fold), Nestin (8.5-fold), Neurog2 (2.8-fold), GFAP (3.5-fold), and NeuroD1 (3.1-fold) (Fig. 5b). Under the stimulus of DO/MM/CUR-loaded NFs in the differentiation medium, the expressions were enhanced for BDNF (13.5-fold), TUBB3 (8.9-fold), and Neurog2 (5.6-fold), and NeuroD1 (5.8-fold). Significantly, the expression levels of Nestin (166-fold) and GFAP (115-fold) were remarkable.

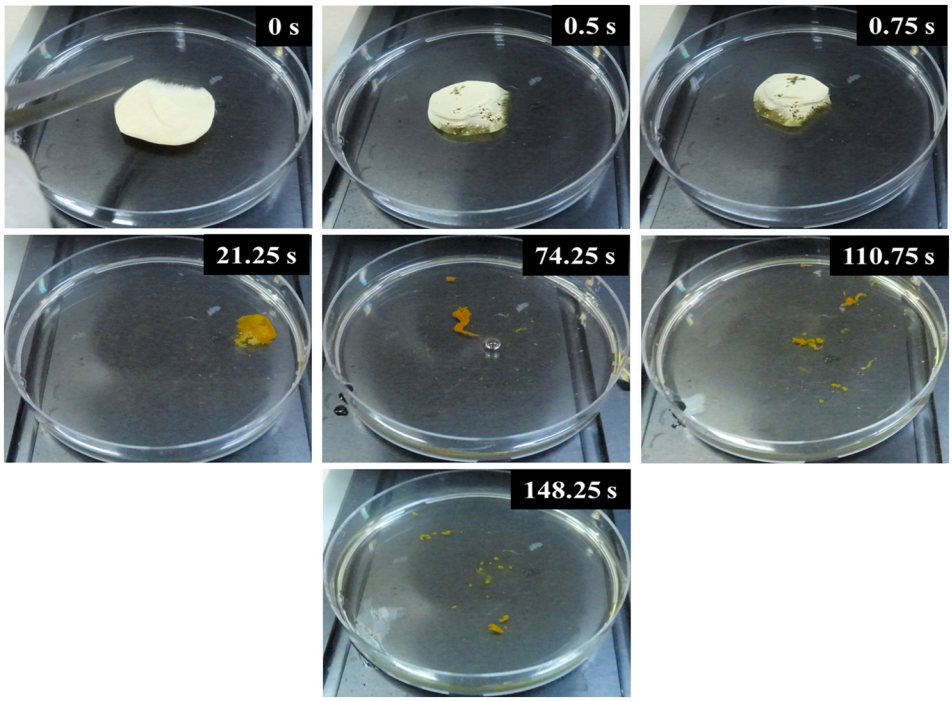

Fig. 2. Images of the DO/MM/CUR-loaded NFs at several time points during the disintegration test.

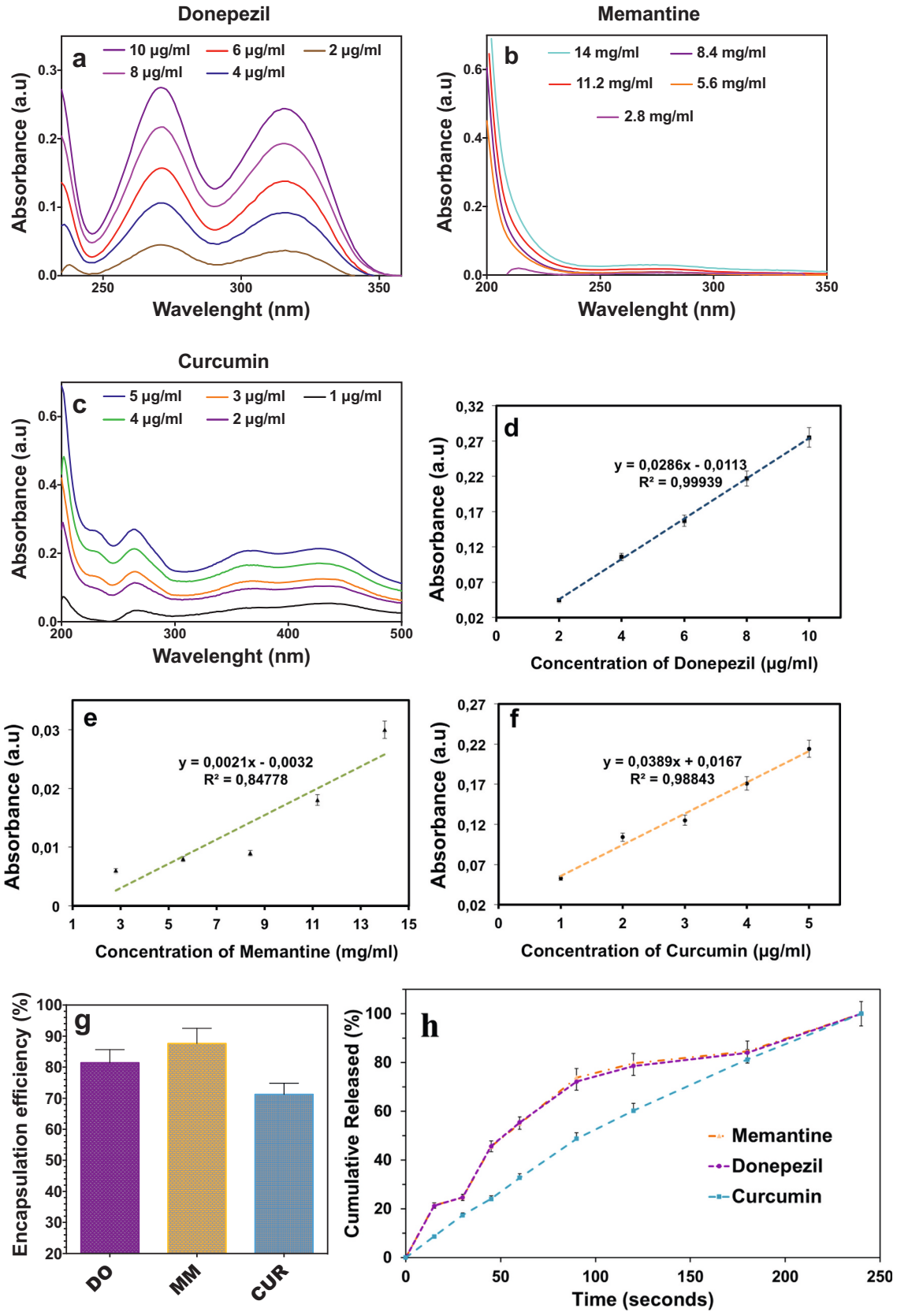

Fig. 3. The *in vitro* dissolution profiles of DO/MM/CUR-loaded NFs: (a) Absorption spectra of donepezil at different concentrations, (b) absorption spectra of memantine at different concentrations, (c) absorption spectra of curcumin at different concentrations, (d) calibration curves of donepezil, (e) calibration curves of memantine, (f) calibration curves of curcumin, (g) encapsulation efficiency of donepezil, memantine, and curcumin, (h) the dissolution profiles of the donepezil, memantine, and curcumin in the DO/MM/CUR-loaded NFs.

Table 3
Mathematical modeling and drug release kinetics of DO/MM/CUR-loaded NFs.

Sample	Korsmeyer-Peppas		Zero Order		First Order		Higuchi		Hixson-Crowell	
	R^2	n	R^2	K_0	R^2	K_1	R^2	K_h	R^2	K_{hc}
DO	0.9599	0.8423	0.8500	0.3820	0.8899	−0.0072	0.9638	6.7894	0.9198	0.0167
MM	0.9597	0.8435	0.9597	0.8435	0.8966	−0.0072	0.9605	6.8350	0.9236	0.0168
CUR	0.9984	0.8555	0.9858	0.4182	0.8369	−0.0072	0.9530	6.8629	0.8910	0.0171

3.12. WST

WST-1 assay was used to test the 24 h-conditioned media's effects in the viability analysis of drugs-loaded and pure NFs on cells. The results indicate that no significant effect of DO/MM/CUR-loaded NFs on fibroblast cells was observed compared to controls. However, the cell viability observed in the pure NFs was statistically more than in the control and DO/MM/CUR-loaded NFs groups ($p < 0.01$) (Fig. 5c).

3.13. Neurobehavioral observations

3.13.1. Locomotion movements

Before starting the neurobehavioral tests, the locomotion abilities of the animals were evaluated with OFT. The results illustrated no significant difference in the latency to enter the center (Fig. 6a) and in square crosses, rearing, and grooming between each group. These results demonstrate that STZ injection and DO/MM/CUR-loaded NFs treatment had no significant effects on autonomous activity (Fig. 6a-e). The data shows that the stereotaxic surgery and administration of drugs had no significant effect on spontaneous locomotion. According to the results of OFT, it is accepted that animals are capable of performing their autonomous activities, and hence, the other behavioral tests can obtain valid results.

3.13.2. Short term memory deficits

NORT was performed to ascertain the effect of DO/MM/CUR-loaded NFs treatment on short-term memory performances. There is an hour between the training and test stages in the NORT. The data obtained at the end of the test stages showed that in the sham group, there is an important difference between the exploration times of familiar and novel objects. ($p < 0{,}001$; Fig. 6f), but there is no difference in the AD group. The rats in the treatment groups spent more time with the novel object than with familiar objects, but there were no considerable differences. According to the test results, differences between the groups were seen in the discrimination index and preferential index values. It was observed that all groups were significantly higher than the AD group in the discrimination index and preferential index (Fig. 6g and h). DO/MM/CUR-loaded NFs administration reversed these high values to the normal levels (Fig. 6g and h). The results yielded an impression that the DO/MM/CUR-loaded NFs treatment improved the short-term memory damage caused by STZ injection.

3.13.3. Passive avoidance test

Rats of different groups did not show a significant difference in initial latency during the acquisition phase. On the contrary, after 24 h, the AD group's step-through latency was significantly lower ($p < 0{,}001$) than the sham group, indicating impaired learning and memory. However, the administration of DO/MM/CUR treatment did not cause a significant change in memory deficits as demonstrated by increased retention latencies (Fig. 6i). The rats treated with DO/MM/CUR-loaded NFs and DO/MM/CUR powder combination could not remember that their presence in the darkroom was related to an aversive stimulus (foot shock).

3.13.4. Morris water maze task

3.13.4.1. Mean escape latency. MWM test consisting of parts including direction determination test and spatial probe test was administered to inspect learning and memory talent. During the acquisition period, the time taken by rats to find the hidden platform decreased gradually, asserting that each group's spatial learning ability was advanced. In terms of mean escape latency, it was observed that there was no significant difference between the groups on the first day. From the second day onwards, the fact that the escape latency of the AD group differed significantly compared to the sham group is interpreted as meaning that the animals in the AD group had low learning skills. In addition, a negligible difference in the value of escape latency was observed between the treatment groups on the second test day. According to the results, the escape latency of rats in the AD group was significantly higher compared to the sham group ($p < 0{,}05$ and $p < 0{,}001$) while DO/MM/CUR-loaded NFs treatment group demonstrated a significant reduction on days 3 and 4 compared to AD group indicating DO/MM/CUR-loaded NFs treatment enhances memory and learning ability (Fig. 7-a).

3.13.4.2. Spatial probe test. The time spent in the target quadrant allows for evaluating the memory performance for the probe trial. Similar effects were seen in the spatial probe test that was performed by removing the platform after the first four days. The spatial probe test made a sign that the crossing platform frequency of rats in the AD group was considerably lower compared to the sham group. DO/MM/CUR-loaded NFs treatment significantly increased the crossing frequency, indicating that DO/MM/CUR-loaded NFs treatment can recover the STZ-induced damage to memory, learning ability, and spatial exploration talent (Fig. 7-b and -c).

3.13.4.3. Path length. The decrease in the path length showing that the animals travel to reach the hidden platform is related to memory. STZ injection demonstrated a significant rise in the path length compared to the sham group throughout the trial period ($p < 0{,}01$).

On the third day, a significant difference was observed in terms of the AD group and treatment groups' path length. DO/MM/CUR-loaded NFs treatment group demonstrated a significant decrease in the path length compared to the AD group ($p < 0{,}001$). DO/MM/CUR powder treatment did not show any significant difference in memory functions compared with NFs treatment in the path length of acquisition trial compared to AD animals (Fig. 7-d). These results showed that NFs treatment improved memory in a supportive manner compared to other parameters. Moreover, there was no significant difference in the swimming speed of rats (Fig. 7-e).

3.14. Biochemical parameters

Our data revealed that amyloid-β levels were significantly elevated in the AD group than in the sham group (Fig. 7-f). Administration of DO/MM/CUR-loaded NFs significantly inhibited the increase of amyloid-β levels in the brain of AD rats. The APP level increased significantly ($p < 0{,}001$) in AD rats compared to the sham group. It showed a more significant decrease in APP levels in DO/MM/CUR-loaded NFs and DO/MM/CUR powder than in the AD group (Fig. 7-g). A significant increase ($p < 0{,}05$) in GSK-3β level was observed in the AD group compared to sham group rats. With DO/MM/CUR-loaded NFs treatment, this increase was reversed and decreased compared to the AD group (Fig. 7-h).

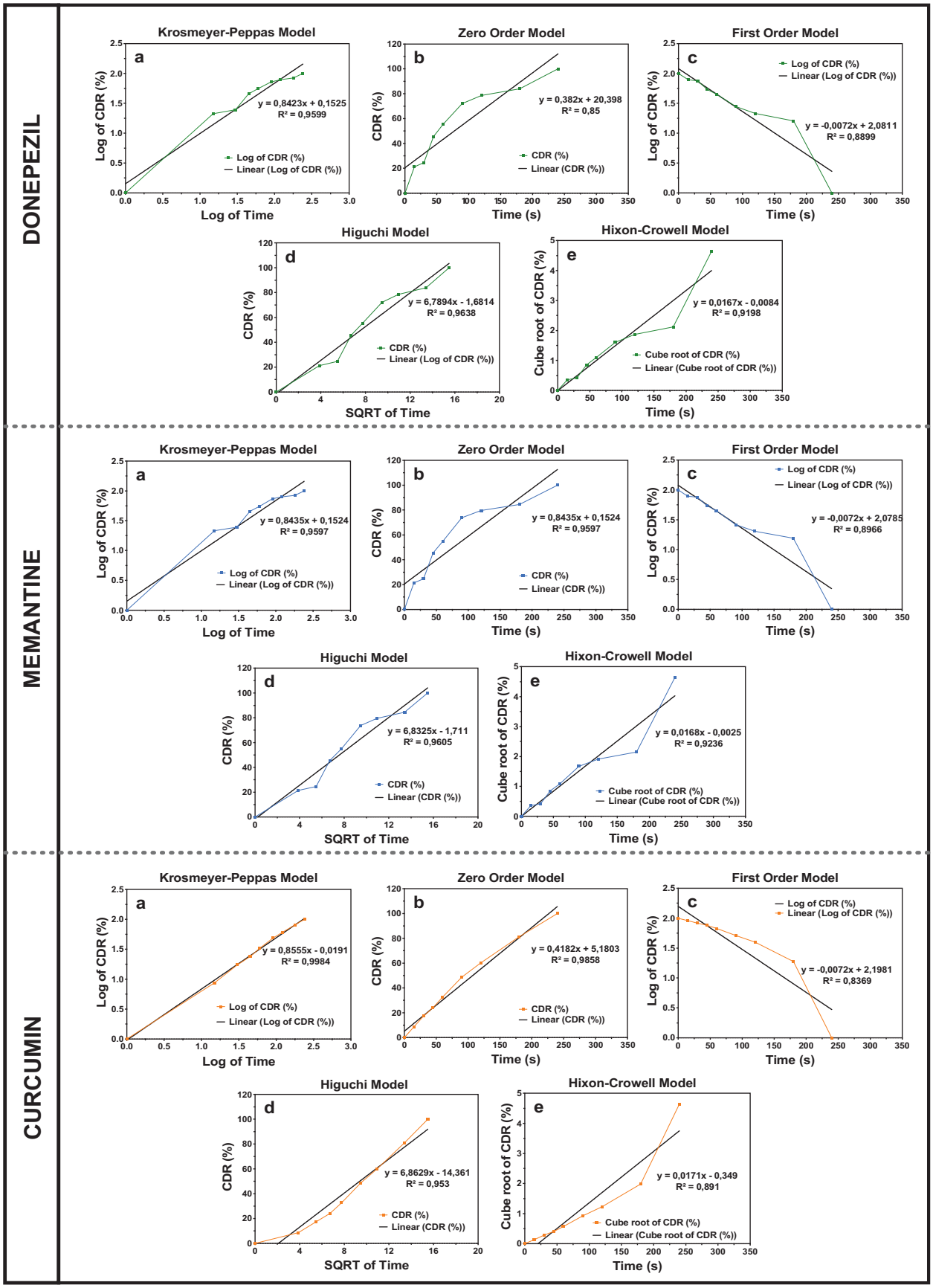

Fig. 4. Analysis of the *in vitro* release kinetics of Donepezil, Memantine, and Curcumin from DO/MM/CUR-loaded NFs with five different mathematical models.

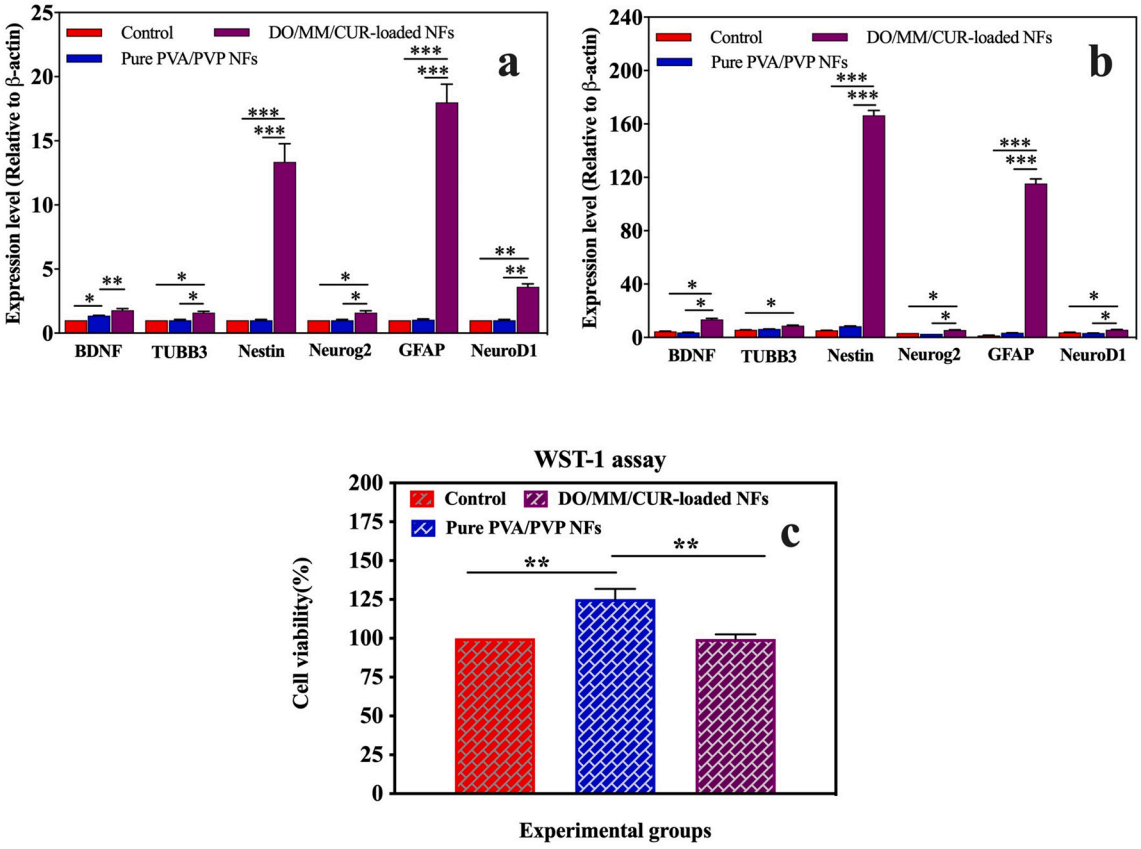

Fig. 5. Gene expression level of neuronal cell markers in DP-SCs in culture medium. The expressions of brain-derived neurotrophic factor (BDNF), glial fibrillary acidic protein (GFAP), Tubb3, Nestin, neuronal differentiation 1 (NeuroD1), and neurogenin 2 (Neurog2) were analyzed after 7 days of culture in the culture medium (a) and the neurogenic differentiation medium (b). WST-1 assay of cell viability (c). Data represent the mean ± standard error of the mean ($n = 3$). Significance differences were found at *$p < 0.05$, ** $p < 0.01$ and *** $p < 0.001$.

In the brains of STZ-treated rats, a considerable rise in AChE levels was observed, compared to a sham group ($p <$ 0,001). However, the increment in AChE levels was significantly improved by DO/MM/CUR-loaded NFs. The effect of DO/MM/CUR powder was similar to that of the nanofiber (Fig. 7-i). A significant difference was found in the hippocampus level of tau between groups (Fig. 7-j). A substantial rise in the level of tau protein was noticed in the hippocampus in STZ-treated rats compared to that in sham rats. However, DO/MM/CUR-loaded NFs treatment ameliorated the STZ-induced increase in tau levels ($p <$ 0,001). The estimated BDNF levels in the AD group's hippocampus had an important drop compared to the sham group ($p <$ 0,05). In addition, DO/MM/CUR-loaded NFs treated animals increased BDNF levels of the hippocampus compared to the AD group, but this increase in BDNF level was not statistically significant (Fig. 7-k). Fig. 7-l showed a significant increase in TNF-α levels of the AD group compared with the sham group. However, no significant differences were seen in DO/MM/CUR-loaded NFs administration compared with the AD group.

3.15. Histopathological analysis

Regular cerebral cortex and hippocampus morphology were observed in the sham group. However, vascular congestion, severe degeneration of neurons, and edema were viewed in the cortex and hippocampus of the AD group. Although neuronal degeneration decreased and regeneration of the hippocampus and cortex increased in the group treated with DO/MM/CUR powder, it was found that the group treated with DO/MM/CUR-loaded NFs was more effective in hippocampus regeneration (Fig. 8).

3.16. Immunohistochemistry analysis

In the icv-STZ model (Fig. 9a-B, F), dense amyloid plaques appeared in the cortex and hippocampus regions of the brain tissues compared to the sham ($p < 0.001$) (Fig. 9a-A, E). In the cortex, reduced immunoreactivity was significantly observed in DO/MM/CUR powder (Fig. 9a-C) and DO/MM/CUR-loaded NFs application (Fig. 9a-D) compared to the AD group ($p < 0.001$ and $p < 0.01$, respectively). In DO/MM/CUR powder (Fig. 9a-G) and DO/MM/CUR-loaded NFs groups (Fig. 9a-H), the hippocampus was rarely positively stained compared to the AD group ($p < 0.05$ and $p < 0.01$, respectively). In comparison to the DO/MM/CUR powder application, it was found that the healing effect of the DO/MM/CUR-loaded NFs was higher in both brain regions. Tau phosphorylation was statistically increased in the cerebral cortex and hippocampal regions in the AD group ($p < 0.001$) (Fig. 9d-B, F) in comparison to sham (Fig. 9d-A, E). However, DO/MM/CUR powder (Fig. 9d-C, G) and DO/MM/CUR-loaded NFs groups (Fig. 9d-D, H) were rarely positively stained compared to the AD group.

4. Discussion

Currently used drugs in Alzheimer's disease (AD) treatment regulate the disease's symptoms. Therefore, these drugs cannot prevent AD but may slow its progression. AD treatment becomes difficult due to the low bioavailability of these drugs that undergo a first-pass effect and side effects resulting from high doses. A sublingual route can be preferred to overcome these problems. This administration route will also allow decreasing the frequency of dosage and increasing patient compliance by giving a single dose instead of multiple medications [53]. According

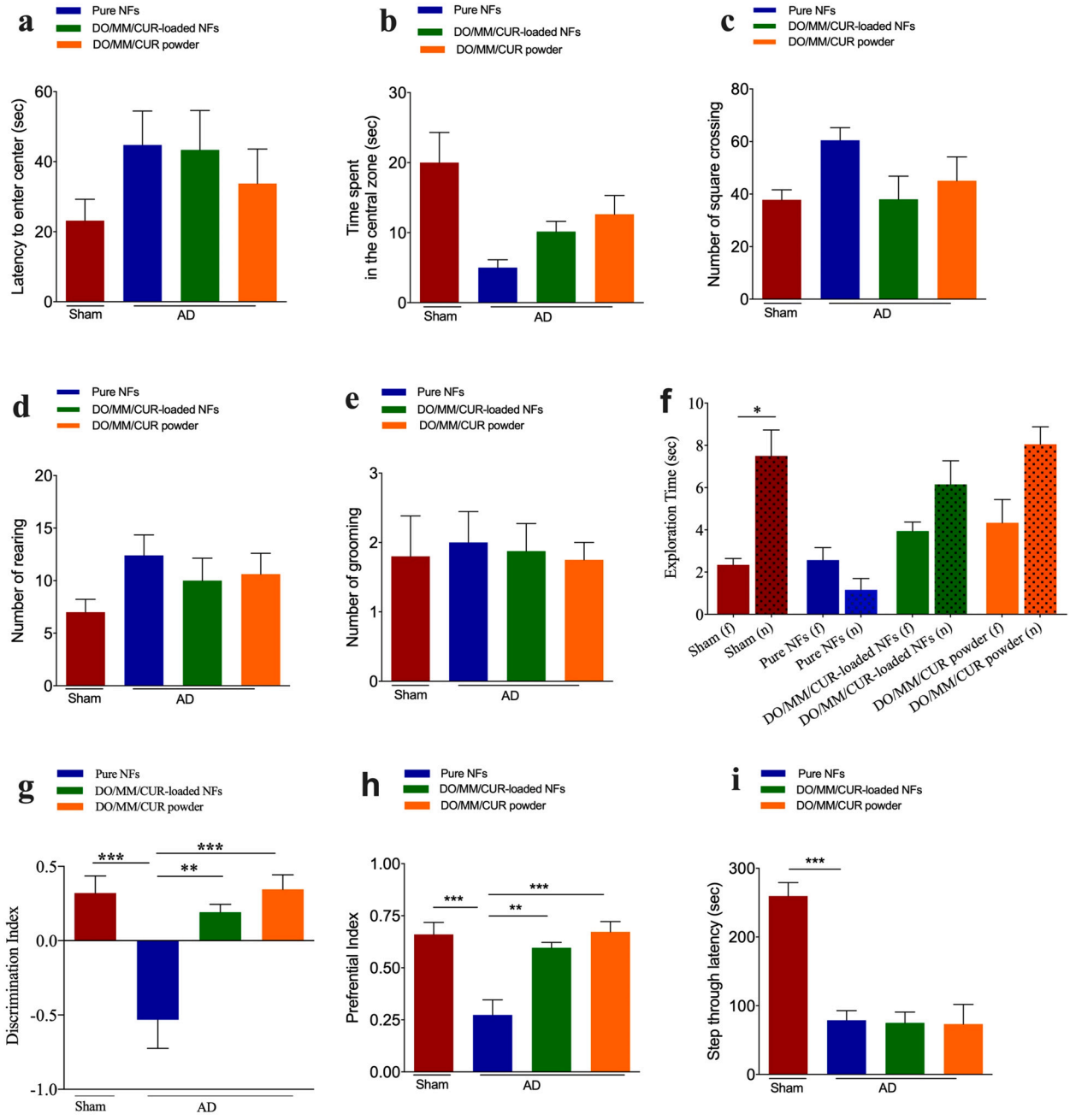

Fig. 6. Effect of DO/MM/CUR-loaded NFs treatment on the autonomous activities and short-term memory of rats with icv-STZ in the open field test (OFT): a) Latency to enter the center, b) time spent in the central zoom, c) number of square crosses, d) number of rearing, and e) number of grooming. Novel object recognition test (NORT): f) Exploration time, g) discrimination index, and h) preferential index. Passive avoidance test (PAT): i) Step-through latency. Data are presented as mean ± standard error of the mean. Significance differences were found at $*p < 0.05$, $** p < 0.01$ and $*** p < 0.001$; f: Familiar, n: Novel.

to recent studies, it is predicted that herbal medicines can be used as supportive care in the treatment of AD [54,55].

This study is the first report that includes the production, characterization, and application of DO/MM/CUR-loaded NFs produced using drugs with different mechanisms of action in AD treatment. In previous studies investigating new treatment strategies for AD, single or two drugs in combination have been generally researched. Also, there are a limited number of studies in which these drugs are formulated with nanotechnological delivery systems [56–59]. CUR-loaded NFs in the study of Guo et al. [60], MM-loaded nanoparticles in the study of Lopez et al. [61], and DO-loaded NFs in the study of AnjiReddy and Karpagam [26] have been successful, however, there is no study involving these three drugs in the literature.

According to SEM images, fibers with the best morphology were produced with the 7:3 ratio of PVA/PVP. It was also seen that surface tension and viscosity are suitable for fibers' production [62]. FT-IR is a spectroscopic method that shows the compounds' chemical structures and interactions between these compounds [63]. According to the FT-IR analysis, the obtained data match the literature data showing the chemical properties of DO/MM/CUR-loaded fibers produced by the electrospinning [41–43,45]. When the XRD results were investigated, while the diffraction patterns of DO, MM CUR, and PVA have shown sharp crystalline peaks, PVP has shown an amorphous profile. DO/MM/CUR-loaded NFs showed a similar profile to pure PVA/PVP NFs but slightly attenuated peaks corresponding to drugs were also observed [46,48,49,64].

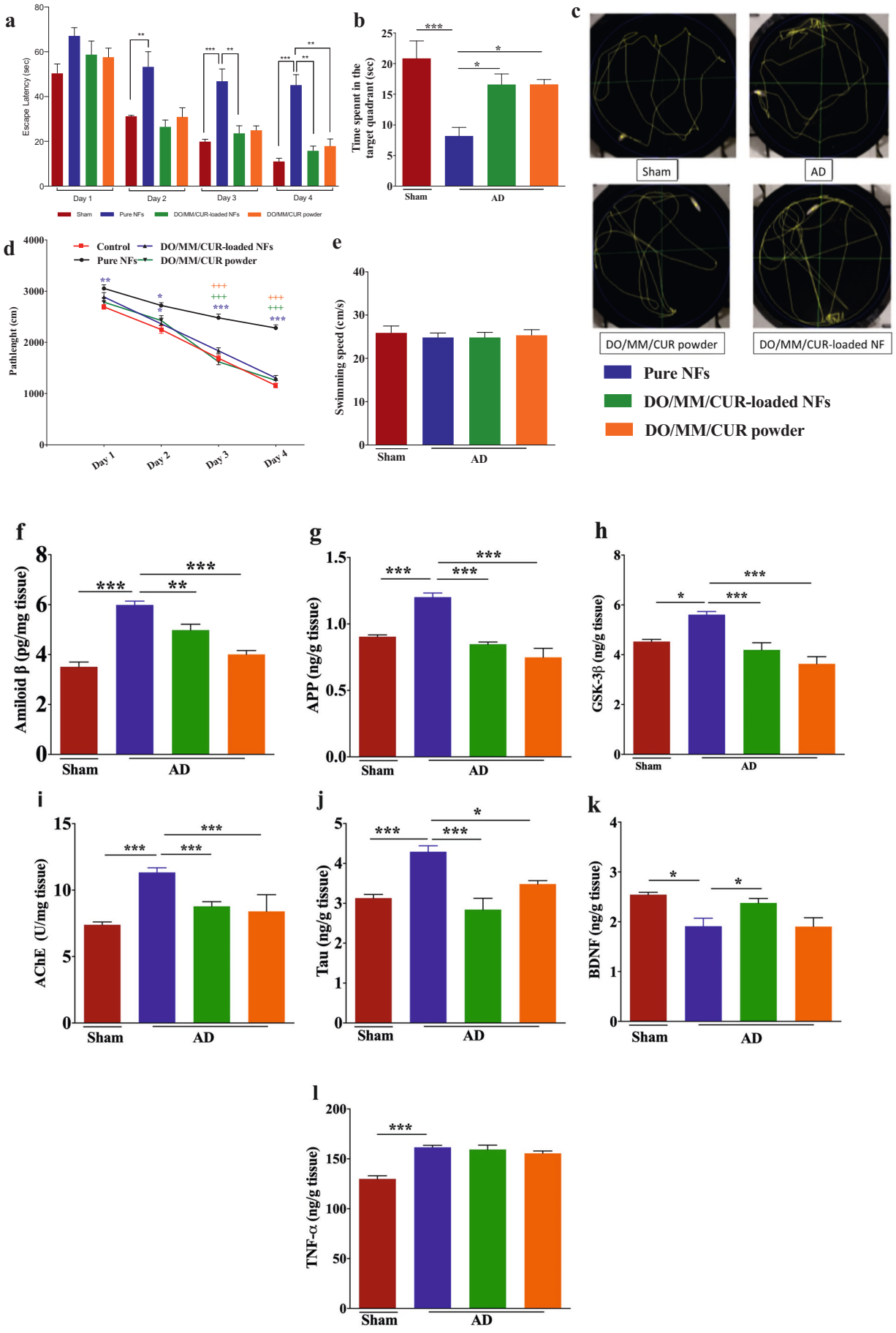

(caption on next page)

Fig. 7. Effects of DO/MM/CUR-loaded NFs treatment on spatial learning and memory function in Morris's water maze: a) Mean escape latency, b) Time spent in target quadrant time, c) The swimming path diagram, d) Path length, and e) Swimming speed. Effects of DO/MM/CUR-loaded NFs treatment on biochemical impacts in the hippocampus of AD rats: f) Amyloid β, g) APP, h) GSK-3β, i) AChE, j) Tau, k) BDNF, and l) TNF-α. Data are presented as mean ± standard error of the mean. Significance differences were found at * $p < 0.05$, ** $p < 0.01$, *** $p < 0.001$.

In the DSC analysis, the Tg and Tm values of the DO/MM/CUR-loaded NFs are lower than that of pure fibers and suggest that there may be physical or chemical interactions between drugs and polymers [65,66]. According to the study by Rajeswari et al. [67], the existence of a single Tg in the DSC curve of PVA/PVP NFs ratifies the miscibility of PVA and PVP polymer. Besides, the working temperature range has been reduced by loading the drugs into the fibers. The reason for this change is a physical or chemical interaction between drugs and polymers. According to the tensile test result, while pure NFs had a rigid and robust structure, they became soft and tough after loading drugs were loaded in NFs. The fibers were suitable for the application although they have been shown to become soft and tough. Rapid wetting and disintegration of drug delivery systems are one of the desired features in the sublingual application used to increase patient compliance. The rapid wetting, disintegration, and dissolution of DO/CUR/MM-loaded NFs suggest that it provides advantages in the sublingual application.

The pure PVA/PVP NFs were found to be compatible with both fibroblast and DP-SCs. The viability of cells in the culture with DO/MM/CUR-loaded NFs was similar compared to the control. In the study by Phan et al. [68], the dose-dependent effect of CUR on fibroblast cells was examined. Herein, while low-dose CUR may be used as a cytoprotective agent against oxidative stress, mild cytotoxic effects were reported in high-dose CUR administration. Similarly, the rapid release of DO/MM/CUR from NFs in this study might indicate a raising of CUR levels to high doses, and CUR's possible cytotoxic effects by adding to NFs have not been observed.

DP-SCs, derived from a cranial neural crest lineage, retain a remarkable potential for neuronal differentiation [69]. DP-SCs express the neural stem cell marker, nestin, which was downregulated upon induction of the differentiation [70]. However, our results indicated that the nestin expression was increased under the differentiation medium's chemical induction effect besides the effect of the drug-loaded NFs. The represented nestin level was expressed as the level relative to the control. The nestin expression in all groups decreased but was much more severe in the control lines. This condition might indicate postponed neuronal differentiation. The other critical alteration in the gene expression profile of the cells is differentiation in the presence of DO/MM/CUR-loaded NFs, which was the level of GFAP, and is a differentiation indicator for the glial cell line. In healthy brain tissue, astrocytes express GFAP but at a low level. Following a neuronal injury, the GFAP level rises significantly [71]. Despite the known function of GFAP in mitosis and cell-cell communication between astrocytes-neurons, its exact function remains unclear. As a result of severe neurodegenerative conditions, glial and fibrous scars might be formed by GFAP-expressing cells. CUR and other drugs packed in NFs could enhance the supportive characteristics of $GFAP^+$ cells while suppressing their roles in the disease onset of AD. The expression of other neuronal markers such as BDNF and TUBB3 also improved. The attenuation of cognitive dysfunction might be explained by the increase of BDNF in the cells.

Memory impairment, learning deficiency, and neuropathological changes, which are symptoms of AD, can be induced in animals by injecting a subdiabetogenic dose of STZ into the ventricles [72]. Administration of STZ creates AD-like effects by decreasing cerebral glucose uptake and insulin receptor expression, disrupting glucose energy metabolism, increasing oxidative damage in the hippocampus, and disrupting neurotransmission in the hippocampus and cortex [53]. Consistent with previous studies, the lack of memory and learning was observed in this study with the application of STZ via the icv, considered to be a successful AD experimental model [73].

The present study investigated the effect of DO/MM/CUR-loaded NFs in preventing memory impairment caused by STZ. The present study results demonstrate that STZ administration caused impairment of working, spatial, and recognition memory, as confirmed by NORT, MWM, and PAT. The findings showed that NFs loaded with DO/MM/CUR have the potential to protect against learning and memory deficits caused by icv-STZ administration.

The NORT results demonstrated that the ability to distinguish similar and new objects decreased in STZ-induced rats, but this reduction was improved with DO/MM/CUR-loaded NFs treatment. In MWM, evaluation of animals during the acquisition session and probe trials displayed a rise in the escape latency and the time spent in the target quadrant of the STZ-treated animals. In the group treated with DO/MM/CUR-loaded NFs, a significant reduction in the time to reach the platform and a decline in time spent in the target quadrant was observed during the acquisition session. Also, the AD group's path length for four days was

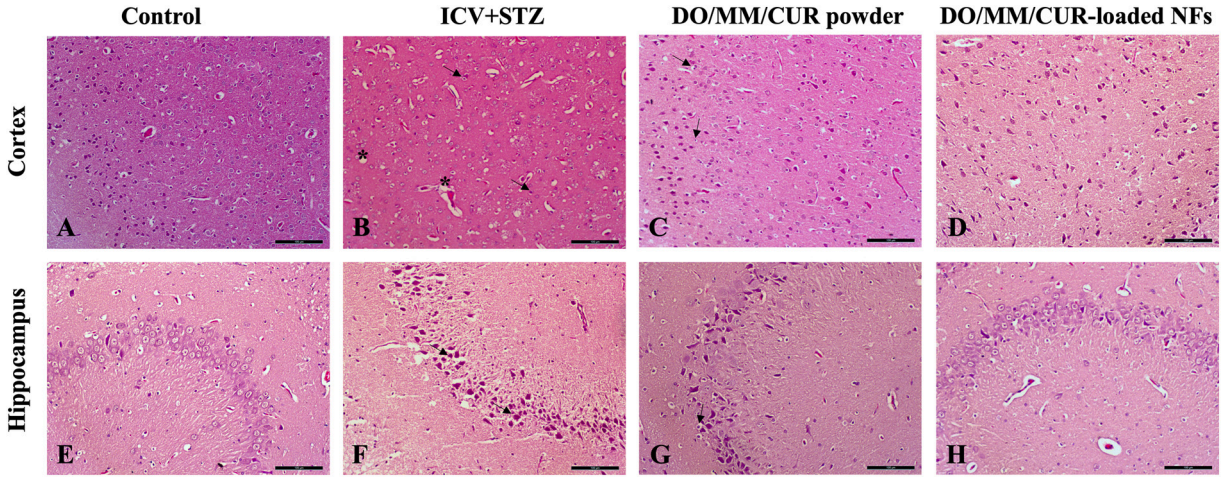

Fig. 8. Photomicrographs of cortex and hippocampus (CA2) regions of brain tissues in experimental groups of rats. A, E: Sham group: regular cerebral cortex and hippocampus morphology; B, F: AD: severe vascular congestion and edema (*) and degenerate neurons (→) in both brain regions; C, G: DO/MM/CUR powder group: mild neuron degeneration (→) in the cerebral cortex and hippocampus; D, H: DO/MM/CUR-loaded NFs group: Similar to normal morphology in the cerebral cortex and hippocampus. Hematoxylin-eosin staining (H&E). Scale: 100 μm.

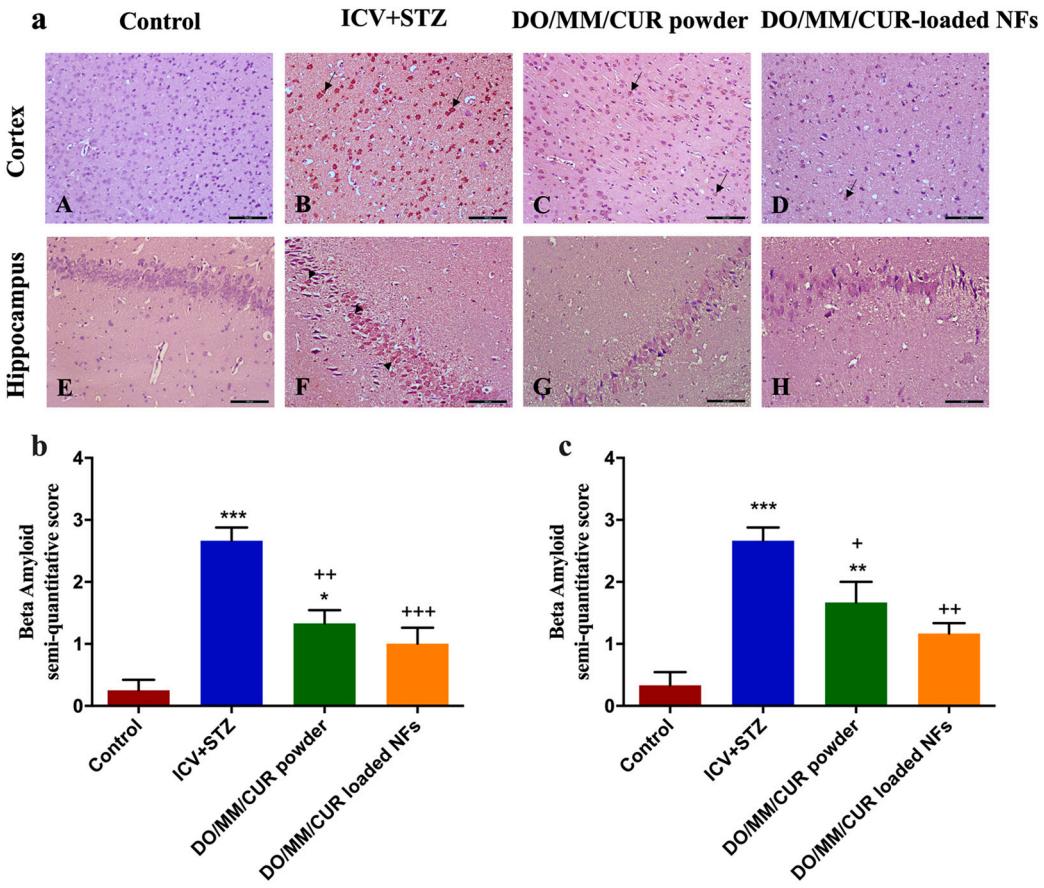

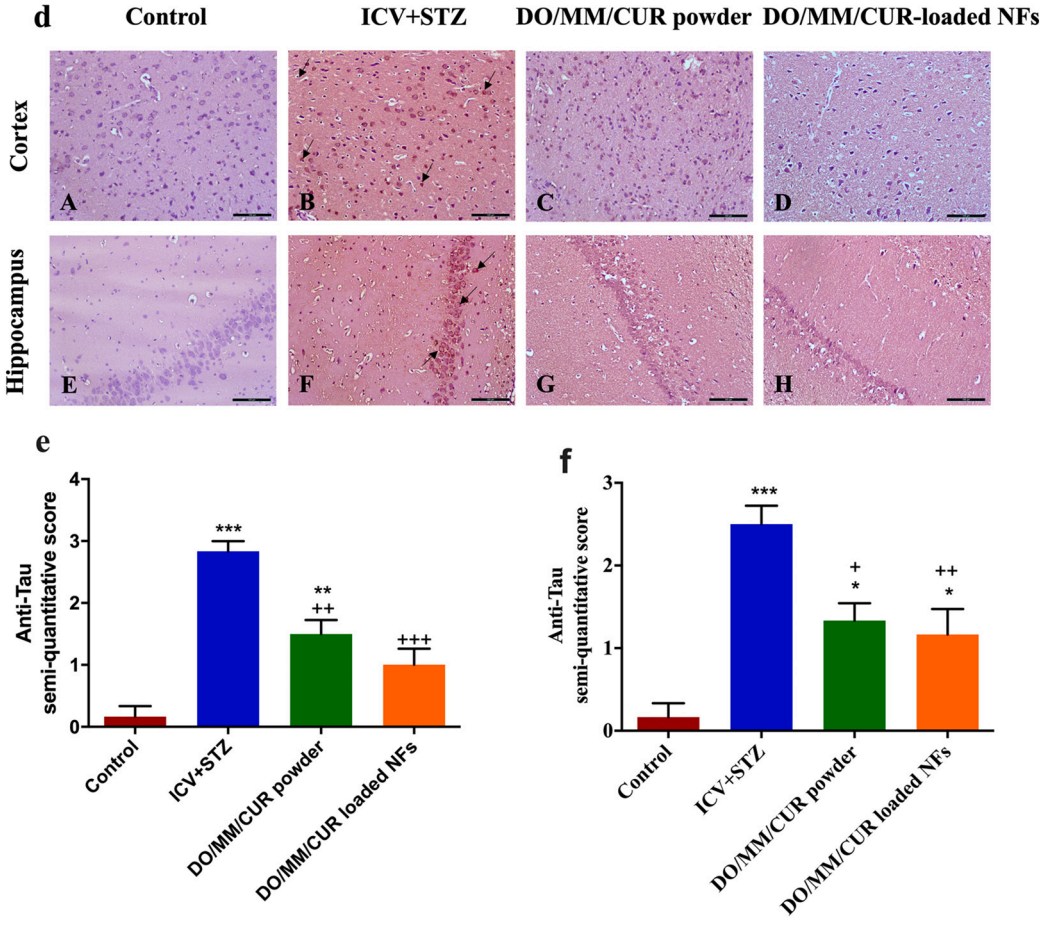

Fig. 9. Immunohistochemical staining of β-amyloid and tau in the cortex and hippocampus (CA2) regions. (Scale 100 μm, $n = 3$ for β-amyloid) a) Increased amyloid plaques in the cortex, and severe immunoreactivity (filled triangles) in the neuronal body in the hippocampus region were observed in the AD (B, F) compared to sham (A, E). It was observed that these plaques ameliorated with the application of DO/MM/CUR powder (C, G) and DO/MM/CUR-loaded NFs (D, H). →: Positive staining. β-amyloid semi-quantitative scoring in the b) cortex and c) hippocampus regions of experimental rat groups. The severe immunoreactivity of anti-tau protein is increased in neural bodies in d) cortex and hippocampus regions of the AD group (B, F) compared to the sham group (A, E) while it is decreased with the application of DO/MM/CUR powder and DO/MM/CUR-loaded NFs (C, G, and D, H, respectively). →: Positive staining. Anti-tau semi-quantitative scoring in the e) cortex and f) hippocampus regions of experimental rat groups. Data are presented as mean ± standard error of the mean. Significance differences were found at *** $p < 0.001$, ** $p < 0.01$, * $p < 0.05$, versus the sham group; $^{+++}$ $p < 0.001$, $^{++}$ $p < 0.01$, $^{+}$ $p < 0.05$ versus the AD group.

considerably higher than the other groups, and the path length of the animals treated with DO/MM/CUR-loaded NFs was close to the sham group animals. Moreover, there was no significant difference between the groups in the animals' swimming speed, which are important for the accuracy of these data during the experiment. The PAT was used for the evaluation of learning and memory deficits in the rats. STZ-administered rats represented a decline in retention latencies in passive avoidance behavior, demonstrating learning and memory impairments. No significant change was observed in animals treated with DO/CUR/MM-loaded NFs compared to animals treated with STZ. In line with these results, treatment of DO/MM/CUR-loaded NFs managed to ameliorate learning loss and memory regression caused by STZ through the neuroprotective effect.

It is widely believed that AD, which is associated with excessive accumulation of abnormal protein structures such as APP, Aβ, and Tau protein, causes structural changes in the brain [74]. According to our data, the increase in the level of Aβ deposition, Tau, and APP caused by STZ induction, which reflects the pathophysiology of AD, was improved with DO/MM/CUR-loaded NFs treatment. Neuropathology caused by the degeneration in the cholinergic system, which plays a significant role in regulating memory and cognition functions, is one of the specific causes of AD [75]. Herein, DO/MM/CUR-loaded NFs significantly inhibit the increase in hippocampal AChE level seen in STZ treated rats due to DO's inhibitory activity at the enzyme level, indicating that there is a possible successful anti-AD activity at a level close to the powder treatment group. Our findings also suggest that memory improved by DO/MM/CUR-loaded NFs therapy can be accounted for, by the decreased level of GSK-3β that has an active role in Tau pathology, a marker of AD [76].

According to the results of histopathological experiments, it was observed that the neuronal degeneration caused by STZ was decreased with DO/MM/CUR-loaded NFs and powder applied to the experimental groups. However, the DO/MM/CUR-loaded NFs were found to be more effective in the regeneration of the cortex and hippocampus compared to the DO/MM/CUR powder group. Furthermore, fewer amyloid plaques and p-tau protein in the cortex and hippocampus were observed in the group of animals receiving the DO/MM/CUR-loaded NFs treatment compared to the group receiving the DO/MM/CUR powder treatment. It can be concluded that the decrease of these amyloid plaques with DO/MM/CUR-loaded NFs shows a much more significant healing effect than powder.

5. Conclusions

In summary, DO/MM/CUR-loaded nanofibers are suitable as a multifunctional nanocarrier system for the combination therapy of AD. In DSC, XRD, and FT-IR studies, it has been shown the drug is completely incorporated into electrospun fibers. DO/MM/CUR-loaded NFs showed appropriate miscibility, rheology, and mechanical and thermal properties. The desired properties for sublingual application were achieved with the fast wetting, dispersion, and dissolution in simulated saliva. The cell viability experiments indicated no cytotoxic effects when the fibroblasts were cultured with NFs. The expressions of BDNF, TUBB3, Neurog2, NeuroD1, Nestin, and GFAP were enhanced by DO/MM/CUR-loaded NFs. DO/MM/CUR-loaded NFs treatment improved the short-term memory damage and enhanced memory, learning ability, and spatial exploration talent according to NORT, OFT, PAT, and MWM in icv-STZ-induced rats. Results indicated that the levels of Aβ, Tau protein, APP, GSK-3β, AChE, and TNF-α were significantly increased, and BDNF was decreased in the STZ-induced rats, while DO/MM/CUR-loaded NFs remarkably reversed their levels compared to the AD group. When the cortex and hippocampus of STZ-induced rat brains were examined histopathologically, neuritic plaques and neurofibrillary nodes are present, whereas rats treated with DO/MM/CUR-loaded NFs did not have this pathology. Fewer amyloid plaques and p-tau protein in the cortex and hippocampus were observed in the group of animals receiving the DO/MM/CUR-loaded NFs treatment compared to the group receiving the DO/MM/CUR powder treatment. According to these results, a new and effective treatment strategy for AD has been developed by increasing bioavailability, decreasing dosage frequency, and increasing patient compliance by giving a single dose from the sublingual route with nanofibers. In conclusion, the sublingual route delivery of DO/MM/CUR-loaded NFs warrants potential clinical application for AD treatment.

CRediT authorship contribution statement

Fadime Topal: Investigation, Methodology, Visualization, Writing-original draft, Writing- review & editing. **Busra Ertas**: Investigation, Methodology, Visualization, Writing- original draft, Writing- review & editing. **Ece Guler**: Resources, Investigation, Methodology, Writing-review & editing. **Fatmanur Gurbuz**: Conceptualization, Resources, Investigation, Methodology. **Gul Sinemcan Ozcan**: Resources, Writing-review & editing. **Oguzhan Aydemir**: Resources, Investigation, Funding acquisition. **Veysel Gokhan Bocekcı**: Resources, Software. **Gokhan Duruksu**: Resources, Writing- review & editing. **Cansun Sahin Cam:** Resources, Writing- review & editing. **Yusufhan Yazir**: Resources, Writing- review & editing. **Oguzhan Gunduz:** Resources, Funding acquisition. **Muhammet Emin Cam**: Conceptualization, Supervision, Writing- original draft, Writing- review & editing, Funding acquisition.

Declaration of competing interest

The authors have no competing interests.

Acknowledgements

Fadime Topal and Busra Ertas contributed equally to this work. This project was supported by a TUBITAK 2209-A Research Projects Program Grant (2209-A, 2019/2, No: 1919B011903601, Scientific and Technological Research Council of Turkey-TUBITAK). We thank Sanovel Pharmaceutical (Istanbul, Turkey), Deva Holding (Istanbul, Turkey), and Joker Food Industry International Domestic and Foreign Trade Company (Istanbul, Turkey) for kindly providing some chemicals and drugs.

Appendix A. Supplementary data

Supplementary data to this article can be found online at https://doi.org/10.1016/j.bioadv.2022.212870. The supplementary data includes the materials and methods for neurobehavioral studies such as open field test, novel object recognition test, passive avoidance test, and Morris's water maze test. A software analysis program and software analysis system were created for this study and the details was added to the supplementary data. Schematic illustration of the methods, schematic extraction procedure of curcumin extract preparation from the *Curcuma longa*, schematic representation in days of the experimental design, image of user interface prepared with ElectronJS, which was used for water maze experiments, physical parameters of solutions, FT-IR spectra of samples, X-ray diffraction patterns of samples, DSC curves of samples, and tensile properties of samples were added as supporting figures in this section.

References

[1] M. Marttinen, et al., Molecular mechanisms of synaptotoxicity and neuroinflammation in Alzheimer's disease, Front. Neurosci. 12 (2018) 963, https://doi.org/10.3389/fnins.2018.00963.

[2] B. Ertas, Beta vulgaris L. var. cicla improves memory deficits in intracerebroventricular streptozotocin injected rats: role on neuroinflammation, Journal of Research in Pharmacy 25 (5) (2021) 589–599, https://doi.org/10.29228/jrp.50.

[3] H. Hampel, et al., The cholinergic system in the pathophysiology and treatment of Alzheimer's disease, Brain 141 (7) (2018) 1917–1933, https://doi.org/10.1093/brain/awy132.
[4] M.D. Hurd, et al., Monetary costs of dementia in the United States, N. Engl. J. Med. 368 (14) (2013) 1326–1334, https://doi.org/10.1056/NEJMsa1204629.
[5] S. Cesur, et al., Electrically controlled drug release of donepezil and BiFeO3 magnetic nanoparticle-loaded PVA microbubbles/nanoparticles for the treatment of Alzheimer's disease, J. Drug Delivery Sci. Technol. 67 (2022), 102977, https://doi.org/10.1016/j.jddst.2021.102977.
[6] J.L. Cummings, G. Tong, C. Ballard, Treatment combinations for Alzheimer's disease: current and future pharmacotherapy options, J. Alzheimers Dis. 67 (3) (2019) 779–794, https://doi.org/10.3233/jad-180766.
[7] W.J. Fessel, Concordance of several subcellular interactions initiates Alzheimer's dementia: their reversal requires combination treatment, Am. J. Alzheimers Dis. Other Dement. 32 (3) (2017) 166–181, https://doi.org/10.1177/1533317517698790.
[8] F. Bisceglia, et al., Prenylated curcumin analogues as multipotent tools to tackle Alzheimer's disease, ACS Chem. Neurosci. 10 (2018), https://doi.org/10.1021/acschemneuro.8b00463.
[9] S.D. Voulgaropoulou, et al., The effect of curcumin on cognition in Alzheimer's disease and healthy aging: a systematic review of pre-clinical and clinical studies, Brain Res. 1725 (2019), 146476, https://doi.org/10.1016/j.brainres.2019.146476.
[10] A. Atri, The Alzheimer's disease clinical Spectrum: diagnosis and management, Med. Clin. North Am. 103 (2) (2019) 263–293, https://doi.org/10.1016/j.mcna.2018.10.009.
[11] Q. Zeng, et al., A combined molecular biology and network pharmacology approach to investigate the multi-target mechanisms of Chaihu Shugan San on Alzheimer's disease, Biomed. Pharmacother. 120 (2019), 109370, https://doi.org/10.1016/j.biopha.2019.109370.
[12] M.L. Toews, D.B. Bylund, Pharmacologic principles for combination therapy, Proc Am Thorac Soc 2 (4) (2005) 282–289, https://doi.org/10.1513/pats.200504-037SR, discussion 290-1.
[13] G.T. Grossberg, et al., Present algorithms and future treatments for Alzheimer's disease, J. Alzheimers Dis. 67 (4) (2019) 1157–1171, https://doi.org/10.3233/jad-180903.
[14] D.-G. Yu, et al., Nanofibers fabricated using triaxial electrospinning as zero order drug delivery systems, ACS Appl. Mater. Interfaces 7 (33) (2015) 18891–18897, https://doi.org/10.1021/acsami.5b06007.
[15] H. Alenezi, M.E. Cam, M. Edirisinghe, Experimental and theoretical investigation of the fluid behavior during polymeric fiber formation with and without pressure, Appl. Phys. Rev. 6 (4) (2019), 041401, https://doi.org/10.1063/1.5110965.
[16] S. Aydin et al n.d.A comparison study of fiber diameter's effect on characteristic features of donepezil/curcumin-loaded polycaprolactone/polylactic acid nanofibers. Macromol. Mater. Eng. n/a(n/a): p. 2100855. doi:10.1002/mame.202100855.
[17] S. Thakkar, M. Misra, Electrospun polymeric nanofibers: new horizons in drug delivery, Eur. J. Pharm. Sci. 107 (2017) 148–167, https://doi.org/10.1016/j.ejps.2017.07.001.
[18] F. Brako, et al., Mucoadhesion of progesterone-loaded drug delivery nanofiber constructs, ACS Appl. Mater. Interfaces 10 (16) (2018) 13381–13389, https://doi.org/10.1021/acsami.8b03329.
[19] F.S. Alfares, et al., Optimization of process-control parameters for the diameter of electrospun hydrophilic polymeric composite nanofibers, Macromol. Mater. Eng. 306 (12) (2021) 2100471, https://doi.org/10.1002/mame.202100471.
[20] Z. Chen, et al., Electrospun nanofibers for cancer diagnosis and therapy, Biomater. Sci. 4 (6) (2016) 922–932, https://doi.org/10.1039/c6bm00070c.
[21] E. Guler, et al., Vitamin D(3)/vitamin K(2)/magnesium-loaded polylactic acid/tricalcium phosphate/polycaprolactone composite nanofibers demonstrated osteoinductive effect by increasing Runx2 via Wnt/β-catenin pathway, Int. J. Biol. Macromol. 190 (2021) 244–258, https://doi.org/10.1016/j.ijbiomac.2021.08.196.
[22] C.S. Easterling, E. Robbins, Dementia and dysphagia, Geriatr. Nurs. 29 (4) (2008) 275–285, https://doi.org/10.1016/j.gerinurse.2007.10.015.
[23] M. Koland, V. Sandeep, N. Charyulu, Fast dissolving sublingual films of ondansetron hydrochloride: effect of additives on in vitro drug release and mucosal permeation, J. Young Pharm. 2 (3) (2010) 216–222, https://doi.org/10.4103/0975-1483.66790.
[24] P. Vrbata, et al., Electrospun drug loaded membranes for sublingual administration of sumatriptan and naproxen, Int. J. Pharm. 457 (1) (2013) 168–176, https://doi.org/10.1016/j.ijpharm.2013.08.085.
[25] T. Potrc, et al., Electrospun polycaprolactone nanofibers as a potential oromucosal delivery system for poorly water-soluble drugs, Eur. J. Pharm. Sci. 75 (2015) 101–113, https://doi.org/10.1016/j.ejps.2015.04.004.
[26] K. AnjiReddy, S. Karpagam, Hyperbranched cellulose polyester of oral thin film and nanofiber for rapid release of donepezil; preparation and in vivo evaluation, Int. J. Biol. Macromol. 124 (2019) 871–887, https://doi.org/10.1016/j.ijbiomac.2018.11.224.
[27] F. Sahne, et al., in: Extraction of Bioactive Compound Curcumin From Turmeric (Curcuma longa L.) Via Different Routes: A Comparative Study 13, 2016, pp. 173–180.
[28] M. Wesierska, J. Svoboda, A. Stuchlik, A therapeutic dose of memantine improves the performance of rats in an active place avoidance task under the continuous dissociation of distal room and proximal arena cues, Neurobiol. Learn. Mem. 162 (2019) 59–66, https://doi.org/10.1016/j.nlm.2019.03.011.
[29] S. Nagasawa, et al., Postmortem redistribution mechanism of donepezil in the rat, Forensic Sci. Int. 266 (2016) 1–7, https://doi.org/10.1016/j.forsciint.2016.04.017.
[30] N. Lamanna-Rama, et al., An update on the exploratory use of curcumin in neuropsychiatric disorders, Antioxidants 11 (2) (2022) 353.
[31] M.E. Cam, et al., A novel treatment strategy for preterm birth: intra-vaginal progesterone-loaded fibrous patches, Int. J. Pharm. 588 (2020), 119782, https://doi.org/10.1016/j.ijpharm.2020.119782.
[32] E. Ilhan, et al., Development of Satureja cuneifolia-loaded sodium alginate/polyethylene glycol scaffolds produced by 3D-printing technology as a diabetic wound dressing material, Int. J. Biol. Macromol. 161 (2020) 1040–1054, https://doi.org/10.1016/j.ijbiomac.2020.06.086.
[33] M.E. Cam, et al., Accelerated diabetic wound healing by topical application of combination oral antidiabetic agents-loaded nanofibrous scaffolds: an in vitro and in vivo evaluation study, Mater. Sci. Eng. C 119 (2021), 111586, https://doi.org/10.1016/j.msec.2020.111586.
[34] M.E. Cam, et al., Fabrication, characterization and fibroblast proliferative activity of electrospun achillea lycaonica-loaded nanofibrous mats, Eur. Polym. J. 120 (2019), 109239, https://doi.org/10.1016/j.eurpolymj.2019.109239.
[35] A. Sri, et al., Preparation of artificial saliva formulation, in: International Conference ICB Pharma, 2015.
[36] M.F.B. Gerzson, et al., Tannic acid ameliorates STZ-induced Alzheimer's disease-like impairment of memory, neuroinflammation, neuronal death and modulates akt expression, Neurotox. Res. 37 (4) (2020) 1009–1017, https://doi.org/10.1007/s12640-020-00167-3.
[37] G. Paxinos, C.R.R. Watson, P.C. Emson, AChE-stained horizontal sections of the rat brain in stereotaxic coordinates, J. Neurosci. Methods 3 (2) (1980) 129–149, https://doi.org/10.1016/0165-0270(80)90021-7.
[38] S. Fanoudi, et al., Everolimus, a mammalian target of rapamycin inhibitor, ameliorated streptozotocin-induced learning and memory deficits via neurochemical alterations in male rats, EXCLI J. 17 (2018) 999–1017, https://doi.org/10.17179/excli2018-1626.
[39] A.K. Sachdeva, et al., Neuroprotective potential of sesamol and its loaded solid lipid nanoparticles in ICV-STZ-induced cognitive deficits: behavioral and biochemical evidence, Eur. J. Pharmacol. 747 (2015) 132–140, https://doi.org/10.1016/j.ejphar.2014.11.014.
[40] M. Overmyer, et al., Astrogliosis and the ApoE genotype. An immunohistochemical study of postmortem human brain tissue, Dement. Geriatr. Cogn. Disord. 10 (4) (1999) 252–257, https://doi.org/10.1159/000017128.
[41] J.K. Park, et al., Controlled release of donepezil intercalated in smectite clays, Int. J. Pharm. 359 (1) (2008) 198–204, https://doi.org/10.1016/j.ijpharm.2008.04.012.
[42] P. Prapatpong, et al., HPLC-fluorescent analysis of memantine: an investigation on fluorescent derivative formation, J. Chem. 2015 (2015) 1–7, https://doi.org/10.1155/2015/672183.
[43] X. Chen, et al., The stability, sustained release and cellular antioxidant activity of curcumin nanoliposomes, Molecules 20 (8) (2015) 14293–14311, https://doi.org/10.3390/molecules200814293.
[44] R. Bryaskova, et al., Synthesis and comparative study on the antimicrobial activity of hybrid materials based on silver nanoparticles (AgNPs) stabilized by polyvinylpyrrolidone (PVP), J. Chem. Biol. 4 (2011) 185–191, https://doi.org/10.1007/s12154-011-0063-9.
[45] M. Abureesh, A. Oladipo, M. Gazi, Facile synthesis of glucose-sensitive chitosan–poly(vinyl alcohol) hydrogel: drug release optimization and swelling properties, Int. J. Biol. Macromol. 90 (2015) 85–90, https://doi.org/10.1016/j.ijbiomac.2015.10.001.
[46] R. Mishra, M. Datt, A. Banthia, Synthesis and characterization of Pectin/PVP hydrogel membranes for drug delivery system, AAPS PharmSciTech 9 (2008) 395–403, https://doi.org/10.1208/s12249-008-9048-6.
[47] Z. Abdeen, S. Mohammad, M. Mahmoud, Adsorption of mn (II) ion on polyvinyl Alcohol/Chitosan dry blending from aqueous solution, Environ. Nanotechnol. Monit. Manag. 3 (2014), https://doi.org/10.1016/j.enmm.2014.10.001.
[48] N. Mittapelly, et al., Investigation of salt formation between memantine and pamoic acid: its exploitation in nanocrystalline form as long acting injection, Eur. J. Pharm. Biopharm. 101 (2016) 62–71, https://doi.org/10.1016/j.ejpb.2016.01.003.
[49] W. Guo, et al., Sustained release donepezil loaded PLGA microspheres for injection: preparation, in vitro and in vivo study, Asian J. Pharm. Sci. 10 (5) (2015) 405–414, https://doi.org/10.1016/j.ajps.2015.06.001.
[50] S. Chauhan, et al., Development, optimization and evaluation of curcumin loaded biodegradable crosslinked gelatin film for the effective treatment of periodontitis, Drug Dev. Ind. Pharm. 44 (7) (2018) 1212–1221, https://doi.org/10.1080/03639045.2018.1439501.
[51] M. Sadri, A. Mohammadi, H. Hosseini, Drug release rate and kinetic investigation of composite polymeric nanofibers, Nanotechnol. Res. J. 1 (2) (2016) 112–121, https://doi.org/10.7508/nmrj.2016.02.008.
[52] P.L. Ritger, N.A. Peppas, A simple equation for description of solute release II. Fickian and anomalous release from swellable devices, J. Control. Release 5 (1) (1987) 37–42, https://doi.org/10.1016/0168-3659(87)90035-6.
[53] M. Moosavi, et al., Effect of carbamylated erythropoietin fc fusion protein (CEPO-Fc) on learning and memory impairment and hippocampal apoptosis induced by intracerebroventricular administration of streptozotocin in rats, Behav. Brain Res. 384 (2020), 112554, https://doi.org/10.1016/j.bbr.2020.112554.
[54] M.-J. Howes, E. Perry, The role of phytochemicals in the treatment and prevention of dementia, Drugs Aging 28 (2011) 439–468, https://doi.org/10.2165/11591310-000000000-00000.
[55] G.Z. Steiner, et al., Study protocol for a randomised, double-blind, placebo-controlled 12-week pilot phase II trial of sailuotong (SLT) for cognitive function in

older adults with mild cognitive impairment, Trials 19 (1) (2018) 522, https://doi.org/10.1186/s13063-018-2912-0.
[56] K. AnjiReddy, S. Karpagam, Chitosan nanofilm and electrospun nanofiber for quick drug release in the treatment of Alzheimer's disease: in vitro and in vivo evaluation, Int. J. Biol. Macromol. 105 (Pt 1) (2017) 131–142, https://doi.org/10.1016/j.ijbiomac.2017.07.021.
[57] G. Calderó, M.J. García-Celma, C. Solans, Formation of polymeric nano-emulsions by a low-energy method and their use for nanoparticle preparation, J. Colloid Interface Sci. 353 (2) (2011) 406–411, https://doi.org/10.1016/j.jcis.2010.09.073.
[58] E. Sanchez-Lopez, et al., Memantine-loaded PEGylated biodegradable nanoparticles for the treatment of glaucoma, Small 14 (2) (2018), https://doi.org/10.1002/smll.201701808.
[59] Z. Aytac, T. Uyar, Core-shell nanofibers of curcumin/cyclodextrin inclusion complex and polylactic acid: enhanced water solubility and slow release of curcumin, Int. J. Pharm. 518 (1–2) (2017) 177–184, https://doi.org/10.1016/j.ijpharm.2016.12.061.
[60] G. Guo, et al., Preparation of curcumin loaded poly(epsilon-caprolactone)-poly (ethylene glycol)-poly(epsilon-caprolactone) nanofibers and their in vitro antitumor activity against glioma 9L cells, Nanoscale 3 (9) (2011) 3825–3832, https://doi.org/10.1039/c1nr10484e.
[61] E. Sánchez-López, et al., Memantine loaded PLGA PEGylated nanoparticles for Alzheimer's disease: in vitro and in vivo characterization, J. Nanobiotechnology 16 (1) (2018), https://doi.org/10.1186/s12951-018-0356-z, p. 32-32.
[62] R.M. Nezarati, M.B. Eifert, E. Cosgriff-Hernandez, Effects of humidity and solution viscosity on electrospun fiber morphology, Tissue Eng. Part C Methods 19 (10) (2013) 810–819, https://doi.org/10.1089/ten.TEC.2012.0671.
[63] R. Paul, E. Genescà, 8 - The use of enzymatic techniques in the finishing of technical textiles, in: M.L. Gulrajani (Ed.), Advances in the Dyeing and Finishing of Technical Textiles, Woodhead Publishing, 2013, pp. 177–198, n/a(n/a).
[64] Z. Abdeen, S.G. Mohammad, M.S. Mahmoud, Adsorption of mn (II) ion on polyvinyl alcohol/chitosan dry blending from aqueous solution, Environ. Nanotechnol. Monit. Manag. 3 (2015) 1–9, https://doi.org/10.1016/j.enmm.2014.10.001.
[65] E. Abdelrazek, I. Elashmawi, S. Labeeb, Chitosan filler effects on the experimental characterization, spectroscopic investigation and thermal studies of PVA/PVP blend films, Phys. B Condens. Matter 405 (2010) 2021–2027, https://doi.org/10.1016/j.physb.2010.01.095.
[66] E. Abdelrazek, et al., Structural, optical, thermal and electrical studies on PVA/PVP blends filled with lithium bromide, Curr. Appl. Phys. 10 (2010) 607–613, https://doi.org/10.1016/j.cap.2009.08.005.
[67] N. Rajeswari, et al., Structural, vibrational, thermal, and electrical properties of PVA/PVP biodegradable polymer blend electrolyte with CH3COONH4, Ionics 19 (8) (2013) 1105–1113, https://doi.org/10.1007/s11581-012-0838-1.
[68] T.T. Phan, et al., Protective effects of curcumin against oxidative damage on skin cells in vitro: its implication for wound healing, J. Trauma 51 (5) (2001) 927–931, https://doi.org/10.1097/00005373-200111000-00017.
[69] V. Mayo, et al., Neural crest-derived dental stem cells–where we are and where we are going, J. Dent. 42 (9) (2014) 1043–1051, https://doi.org/10.1016/j.jdent.2014.04.007.
[70] M. Takeyasu, T. Nozaki, M. Daito, Differentiation of dental pulp stem cells into a neural lineage, Pediatr. Dent. J. 16 (2) (2006) 154–162, https://doi.org/10.1016/S0917-2394(06)70081-7.
[71] J.D. Alibhai, A.B. Diack, J.C. Manson, Unravelling the glial response in the pathogenesis of Alzheimer's disease, FASEB J. 32 (11) (2018) 5766–5777, https://doi.org/10.1096/fj.201801360R.
[72] P. Shahmohamady, et al., Effect of sinapic acid on memory deficits and neuronal degeneration induced by intracerebroventricular administration of streptozotocin in rats, Pol. J. Pathol. 69 (2018) 266–277, https://doi.org/10.5114/pjp.2018.79546.
[73] T. Guardia de Souza e Silva, Oral treatment with royal jelly improves memory and presents neuroprotective effects on icv-STZ rat model of sporadic Alzheimer's disease, Heliyon 6 (2) (2020), e03281, https://doi.org/10.1016/j.heliyon.2020.e03281.
[74] S. Raheja, et al., Aegle marmelos leaf extract ameliorates the cognitive impairment and oxidative stress induced by intracerebroventricular streptozotocin in male rats, Life Sci. 221 (2019) 196–203, https://doi.org/10.1016/j.lfs.2019.02.032.
[75] H.E. Mohamed, et al., Raspberry ketone preserved cholinergic activity and antioxidant defense in obesity induced alzheimer disease in rats, Biomed. Pharmacother. 107 (2018) 1166–1174, https://doi.org/10.1016/j.biopha.2018.08.034.
[76] A. Akhtar, M. Bishnoi, S.P. Sah, Sodium orthovanadate improves learning and memory in intracerebroventricular-streptozotocin rat model of Alzheimer's disease through modulation of brain insulin resistance induced tau pathology, Brain Res. Bull. 164 (2020) 83–97, https://doi.org/10.1016/j.brainresbull.2020.08.001.